Optimal Demand Response Resource Exploitation for Efficient Accommodation of Renewable Energy Sources in Multi-Energy Systems Considering Correlated Uncertainties

Bo Zeng[a], Yu Liu[a], Fuqiang Xu[a], Yixian Liu[a], Xiaoyan Sun[b], Xianming Ye[c]

a. State Key Laboratory of Alternate Electrical Power System with Renewable Energy Sources, North China Electric Power University, Beijing 102206, China

b. School of Information and Control Engineering, China University of Mining and Technology, Xuzhou 221116, China

c. Department of Electrical, Electronic, and Computer Engineering, University of Pretoria, Pretoria 0002, South Africa

Abstract

This paper proposes a comprehensive planning model for enhancing accommodation of renewable energy sources into a combined heat and power based multi-energy system by utilizing the flexibility of a demand response program. As distinct from existing works, demand response has been implemented through a price-based program not only in terms of its effects on system operation but also for the planning decisions, and the potential correlations among uncertainties (i.e., renewable energy sources availability, load demand, and demand-side responsiveness) have been explicitly considered in our study. The concerned problem is interpreted into a two-stage optimization problem, where the placement of advanced metering infrastructures, the installation of renewable generation units along with the relevant pricing strategy for the demand side are jointly optimized to minimize the overall economic costs of the system. The flexibility of customers' energy demands in response to real-time price changes is represented by using a generalized elasticity model, through which the demand response in terms of both load shifting in the temporal dimension, and the switching of energy source on the demand side can be properly captured under a unified framework. An efficient scenario generation method leveraging a series of correlation-handling techniques is employed to address the uncertainties in the proposed problem and a comprehensive scenario reduction method based on a novel optimal clustering technique is further introduced to alleviate the computational burden of the resultant model with the correlated uncertainties. Compared with the existing literatures, the novelty of this paper is in three-fold: 1) This study investigates the potential value of demand response for promoting renewable energy exploitation from a long-term planning perspective, instead of the conventional operation aspect. 2) The impacts from both system uncertainties and their potential correlations have been explicitly considered. 3) A comprehensive scenario reduction method based on

optimal clustering analysis is introduced and employed to alleviate the solving complexity and improve the computational efficiency of the proposed model. The proposed planning framework is demonstrated on an illustrative test case and the simulation results verified the effectiveness of the developed model.

Keywords: renewable energy; multi-energy system; demand response; advanced metering infrastructure; correlated uncertainties; planning

Nomenclature

Acronyms

AMI	Advanced metering infrastructure
CHP	Combined heat and power
CL	Critical load
DR	Demand response
ECL	Energy-convertible load
MES	Multi-energy system
MESO	MES operator
OUT	Out sample stability
RES	Renewable energy source
RTP	Real-time price
SP	Stochastic programming
TSL	Time-shiftable load
WTG	Wind turbine generator

Indices (Sets)

i/Ω_I	System buses
w/Ω_w	Candidate locations for installation of renewable energy generation units
d/Ω_d	Candidate locations for installation of AMI unites
s/Ω_s	Uncertainty scenarios
t/T	Time periods
type	Customer sector

Parameters

τ	Annualization factor
α	Discount rate (%)
β	Weight coefficient used in scenario reduction
$\lambda_{min}/\lambda_{max}$	Lower/upper bound
θ	Number of typical days in a year
ζ	Service life (year)
cc	Capital cost of equipment ($)
cm	Maintenance cost in a year ($)
$N^{household}$	Number of candidate load points
P^{WTG-r}	Rated output power of a WTG (kW)
P^{CHP-r}	Rated output power of CHP (kW)
$P^{Trans-r}$	Rated output power of a transformer (kW)
σ^{GR}	Price of procuring power from the external grid ($/kWh)
σ^{GS}	Price of procuring gas from gas station ($/m^3)
$\rho^{e,0}/\rho^{h,0}$	Electricity/heat tariff price under regular case ($/kWh)
p	Probability of scenarios
η	Energy conversion efficiency
γ	Heat-to-electric ratio
HV	Heat value of natural gas
$v^{in}/v^{ra}/v^{out}$	Cut-in/rated/cut-out wind speed (m/s)
$\mathbb{C}_X$	Spearman correlation coefficient matrix of random variables $X_i\,(i = 1, \ldots, n)$
κ_{ij}	Correlation coefficient between random variables X_i and X_j in $\mathbb{C}_X$

Variables

OF	First-stage objective ($)
OS	Second-stage objective ($)
IC	Investment cost ($)
MC	Maintenance cost ($)
EP	Energy procurement cost ($)

RE	Revenue loss of MESO due to DR program ($)
χ	AMI penetration rate (%)
n	Number of installed components
P^{GR}	Amount of power procured from the external market (kW)
G^{GS}	Amount of gas procured from the external market (m^3)
ρ^e/ρ^h	Real-time electricity/heat price offered to customers ($/kWh)
v	Wind speed (m/s)
$P^{CHP}/P^{Trans}/P^{WTG}$	Active output power of CHP/transformer/WTG (kW)
$Q^{CHP}/Q^{Trans}/Q^{WTG}$	Reactive output power of CHP/transformer/WTG (kVar)
H^{CHP}	Heat output of CHP (kW)
G^{CHP}	Amount of natural gas consumed by CHP (m^3)
D	Total system demand (kW)
PD/QD	Active/reactive power demand (kW)
HD	Heat demand (kW)
ε^{TL}	Own elasticity of TSLs
ϵ^{TL}	Cross elasticity of TSLs
ε^{EL}	Own elasticity of ECLs
ϵ^{EL}	Cross elasticity of ECLs

1. Introduction

Climate change and environmental crises provide a strong impetus for energy systems to transform toward low-carbon and sustainable prospects (Batel et al., 2013). Accordingly, the concept of multi-energy system (MES) including multiple energy carriers based on combined heat and power (CHP) generation technology has been suggested and has attracted increasing attention in recent years (Linna et al., 2007). Unlike conventional generation units, CHP produces electricity with synchronous utilization of the exhaust heat during the process of power generation. This feature endows CHP systems with the possibility to boost the overall efficiency of energy usage while reducing the greenhouse gas emissions due to the primary energy savings requested for heat supply (Andersen and Lund, 2007). Because of this, the proportion of

CHP in the generation mix of many countries has been steadily increasing in recent decades (Benam et al., 2015).

Despite the significant benefits presented above, the extensive adoption of CHP, however, tends to incur additional complexities/challenges for future energy systems because of its reduced flexibility during operation (Shao et al., 2018). Specifically, the output power of CHP units is limited by the heat output ; thus, to cope with the fluctuation in customer energy demands, utilities have to rely heavily on operating reserve (procurement of ancillary services) to fulfil the requirement of power balance, and this limit dramatically depresses the profit of MES operator (MESO). Furthermore, with developing penetration level of renewable energy sources (RESs) in the MES, the above limitation also leads to severe RES curtailment in some periods when the power production of CHP is at the peak and covers most of the customer electricity demand.

To properly resolve the challenge of RES integration into CHP-based MESs, a great number of researches have been dedicated to mitigating the coupling of electricity and heat carriers for such system, among which demand response (DR) is one of the most suggested solutions (Papadimitriou et al., 2019).

Since the operation of CHP is limited by the production of heat output, encouraging customers to change their energy consumption patterns (particularly heat demand) in response to real-time supply conditions can be a viable means to improve the operational performance of CHP-based systems. In the context of an MES, customers have possibilities to implement DR through different energy carriers due to the proliferation of "advanced metering infrastructure (AMI)" on the demand side (Eissa, 2019). Such inherent flexibility enables customers to behave actively and interact with the MES by not only adjusting the timing of their consumption but also switching the sources of the energy they use to fulfill their requirements (Wang et al., 2017). In this respect, with such demand-side "responsiveness", the heat-electricity coupling constraints of CHP could be released to some extent, and the MESO could be provided with additional balancing resources for coping with the volatility of system operation and accommodating RESs in the CHP-based MES.

In recognition of the above fact, a growing number of studies have recently focused on the DR integration problem in MESs. For example, DR was considered as a control measure by (Dolatabadi and Mohammadi-Ivatloo, 2017) and energy flow-based analyses were conducted to examine the impacts of DR on MES efficiency with respect to technical and economic metrics. An automated energy management system based on a reinforcement learning algorithm is presented in (Sheikhi et al., 2016) to motivate

residential customers for participating in DR programs in a CHP-based MES. Also, considering the dynamic characteristics of DR management, (Zhang et al., 2020) proposed an interval optimization based coordination scheduling model for a gas–electricity coupled system, while in (Zeng et al., 2019), the conventional electricity-based DR concept in smart grids was extended for multi-energy settings, and the potential benefits resulting from energy substitution were quantitatively estimated. (Zhang et al., 2016b) presented an optimal probabilistic scheduling model for MESs with consideration of the DR effect. The optimal DR control strategy for maximizing the total expected social welfare and facilitating market participation was investigated. (Liu et al., 2018a) reported a comprehensive framework to incorporate the DR potential of smart buildings in MES operations. In addition, a mixed-integer nonlinear programming model for the operation management of an MES with RESs and price-based DR was developed by (Zeng et al., 2014), wherein the optimal pricing scheme for enhancing RES integration was studied while considering the carbon footprint. To properly estimate the DR capability of customers under an interactive environment, a bilevel modeling framework based on a game theoretic method was proposed by (Liu et al., 2018b), and the effects of DR on the operating performance of an MES were quantified through a comparative analysis. Based on this foundation, an extended study was conducted by (Qadrdan et al., 2017), this paper proposed an ordinal potential game model to access benefits brought by DR for different participants. Finally, (Pan et al., 2019) presented an MES planning and operation co-optimization model with DR. In their work, customers' energy demands were assumed to be directly managed by the MESO, and a novel flow-tracing approach was used to determine the optimal nodal energy pricing strategy that improves system operation security and reduces corresponding costs.

In all the works presented above, it can be seen that the integration of DR would bring about significant benefits to an MES if utilized properly. However, for most extant literatures, the presented investigations have merely focused on the issues of DR at the operation level rather than from a planning perspective.

Nevertheless, in reality, activating DR implies the need for extra investment in AMI to enable two-way communication between the MES and customers; thus, the implementation of DR in the MES may lead to a rise in the total investment/operating costs and exploring the optimal solution of AMI placement is essential for the MESO to make the most of the benefits from the DR program. Therefore, more research about such problems should be conducted from a planning perspective.

In addition, in all the studies presented above, it has been assumed that the MESO always had complete knowledge of the demand responsiveness of its customers; thus, the potential uncertainties associated with

DR were ignored (Kim and Norford, 2017) or simply described using an independent probabilistic model (Pazouki and Haghifam, 2016). In practice, such DR models might be suitable for some specific applications (e.g., a direct load control (DLC)-based DR program (Zhang et al., 2016a) in which customers cannot decide whether to respond to DR when receiving calls from the system), but they might no longer be applicable in future market settings, as DR might be solicited via a non-direct control program, e.g., real-time pricing (Liu et al., 2018a), or time-of-use tariff (Rastegar et al., 2015). Specifically, under the non-direct-control DR program, MES customers have the freedom to set their energy consumption patterns (Bahrami and Sheikhi, 2016) and decide how to respond to DR-induced signals according to their own preferences (Sheikhi et al., 2015); thus, the introduction of DR may significantly increase the uncertainties in MES operation (Shao et al., 2018).

Owing to the randomness in the RES supply (Mehrjerdi and Rakhshani, 2019), the power output of renewable energy generation tends to be highly stochastic during operation. Also, the load demand of the system could be uncertain, arising from either the inherent volatility in customer consumption or load forecasting inaccuracy (Mehrjerdi, 2020).

In actual implementations, as the outputs of renewable energy generation, load demand, and customer responsiveness are time dependent, there might exist a high degree of correlation among these uncertainties. The existence of such correlations has a considerable impact on the operational performance of the system (Mehrjerdi and Hemmati, 2020). Therefore, implementing DR without proper consideration of its stochastic features and potential correlations with the other random factors may lead to suboptimal or even infeasible planning decisions for the MESO. Although the uncertainty modeling of DR has been widely discussed in extant literatures, e.g., (Neyestani et al., 2015), barely any of them have noticed the issue of correlations among uncertainties in the context of MES planning, hitherto.

Table 1 Comparison of Proposed Work with Existing Literatures

Reference	DR program	Uncertainty			Correlation consideration
		RES	Load demand	Demand-side responsiveness	
(L. Gan et al., 2016)	×	×	×	×	×
(Jangamshetti and Rau, 2001)	×	×	×	×	×
(Qin et al., 2013a)	×	×	×	×	✓
(Zhang et al., 2018)	×	✓	✓	×	✓
(Mehrjerdi, 2020)	×	✓	✓	×	×
(Mehrjerdi and Rakhshani, 2019)	×	✓	✓	×	×
(Qadrdan et al., 2017)	✓ (DLC)	×	×	×	×

(Mehrjerdi and Hemmati, 2020)	✓ (DLC)	✓	×	×	×
(Zhang et al., 2016a)	✓ (DLC)	✓	✓	×	×
(Pazouki and Haghifam, 2016)	✓ (DLC)	✓	✓	×	×
(Zhang et al., 2016b)	✓ (DSB)	×	✓	×	×
(Zhang et al., 2020)	✓ (DLC, TOU)	×	×	×	×
(Eissa, 2019)	✓(RTP)	×	×	×	×
(Pan et al., 2019)	✓(RTP)	×	×	×	×
(Bahrami and Sheikhi, 2016)	✓(RTP)	×	×	×	×
(Sheikhi et al., 2015)	✓(RTP)	×	×	×	×
(Rastegar et al., 2015)	✓(TOU)	×	×	×	×
(Liu et al., 2018b)	✓(DSB)	×	×	×	×
(Shao et al., 2018)	✓(DSB)	×	×	×	×
(Liu et al., 2018a)	✓(RTP)	×	×	×	×
(Sheikhi et al., 2016)	✓(RTP)	×	×	×	×
(Kim and Norford, 2017)	✓(RTP)	✓	×	×	×
(Dolatabadi and Mohammadi-Ivatloo, 2017)	✓(RTP)	✓	✓	×	×
(Neyestani et al., 2015)	✓(CB)	×	×	✓	×
(Zeng et al., 2019)	✓(RTP)	✓	✓	✓	×
(Zeng et al., 2014)	✓(RTP)	✓	×	✓	×
Proposed model	**✓(RTP)**	✓	✓	✓	✓

*Direct load control (DLC), demand side bidding (DSB), real-time pricing (RTP), time-of-use tariff (TOU), carrier-based pricing (CB)

To address the above knowledge gaps, a new methodological framework is proposed for enabling CHP-based MESs to accommodate the growing penetration of RESs by utilizing the DR solution. In sharp contrast to most extant works, the present study considers customers' flexible demands as an additional balancing resource for mitigating the difficulty of RES integration with CHP-based MESs and aims to provide the most efficient strategy for exploiting such potential from *a planning perspective*. To fit future market settings, the DR in our research is modeled as price-dependent demands characterized by the price elasticities instead of the conventional direct load control program. In this regard, introducing the price-based DR into MES entails the investment in AMI which results in the problem to be a two-stage optimization program — *the placement of AMI and the relevant pricing strategy for the demand side are jointly optimized along with the allocation of renewable generation units to minimize the overall economic costs of the system*. The proposed model is developed through a scenario-based stochastic programming formulation to explicitly capture the correlations among uncertainties (i.e., customers' varying responsiveness, energy demand, and RES generation) in long-term planning studies. To solve the proposed model, a comprehensive scenario generation and reduction method based on optimal clustering analysis is

employed to address the correlated uncertainties involved in the problem. The main difference between the proposed work and the existing studies in the related field is summarized in Table 1.

The main contributions/innovations of this paper are highlighted as follows:

1) **An original DR resource planning framework to accommodate the growing penetration of RESs in CHP-based MESs is proposed**. The impact of DR for RES exploitation is investigated in an MES planning setting (rather than an operation context), where AMI is innovatively considered as a strategic flexibility resource and taken into account the long-term investment decision of MESs. With the proposed framework, the decision-maker can determine the "real value" by performing price-based DR in an RES-integrated MES expediently, in terms of not only its effects for system operation but also investment decisions. In this light, depending on the context of practical applications, the proposed framework may provide a scientific tool by informing the current debates about the role of DR in future MES planning and market development. Undoubtedly, this would be helpful for MESOs to make optimal investment decisions and properly utilize the potential benefits of the DR program in the planning stage.

2) **Potential correlations among uncertainties for multi-energy system operation (i.e., renewable energy sources availability, load demand, and demand-side responsiveness) have been explicitly considered**. In contrast to the most previous works, both the uncertainties of customer performance (responsiveness) in the price-based DR program and their potential correlations with respect to other random factors (RES output and load demand) have been explicitly captured in this study. These considerations distinguish the present work and make our model capable of yielding a more realistic and comprehensive representation of the characteristics as they occur in reality, and would lead to more convincing planning results than existing studies.

3) **A comprehensive scenario reduction method based on optimal clustering analysis is introduced and employed to alleviate the solution complexity and improve the computational efficiency of the proposed model**. The suggested framework introduces a correlation loss concept to address the problem of correlation deviation in high-dimensional scenario reductions. As such, it is fundamentally different from the conventional distance-based scenario reduction methods and could exhibit better performance in preserving the sample stability (statistical consistency) of stochastic programming (SP) under correlated uncertainties and shows greater validity in practical applications.

2. Problem Statement

The structure of the MES under discussion in this study is shown in Fig. 1. The concerned MES is a typical distribution-level MES that consists of multiple CHP units, whose input ports are connected to the external power/gas networks while its outputs link the electricity and heat demands of end customers.

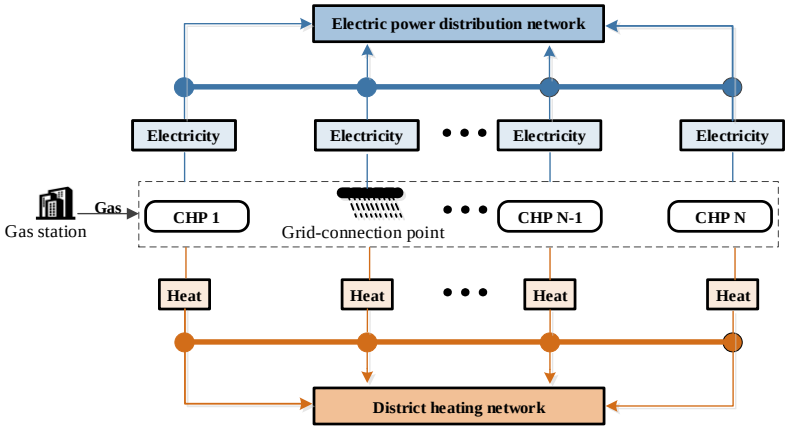

Fig. 1. General Structure of Distribution-level MES

In this study, it is assumed that the discussed MES is owned and managed by the same entity, that is, MESO. As a private self-interested entity, the objective of the MESO is to supply the energy demands of MES customers with the lowest total cost by efficient integration of RESs. To achieve this, DR is utilized and implemented by the MESO through a real-time price (RTP)-based program. In the RTP, the MESO depends on time-variant pricing signals to solicit the DR of customers by using two-way communication equipment AMI.

However, as equipping the MES with AMI requires extra investment and the performance of DR can be largely dictated by the "nature" of customers (load characteristics, consumption pattern, price sensitivity, etc.), for the MESO, there is a great need to analyze different AMI configuration plans (i.e., DR resource exploitation strategies) at the demand side and evaluate their costs and benefits (economic efficiency) through investigating the MES operation over the planning horizon. Optimal AMI planning aims to enhance RES exploitation and minimize the overall cost of the energy supply subject to the various operating constraints of the system.

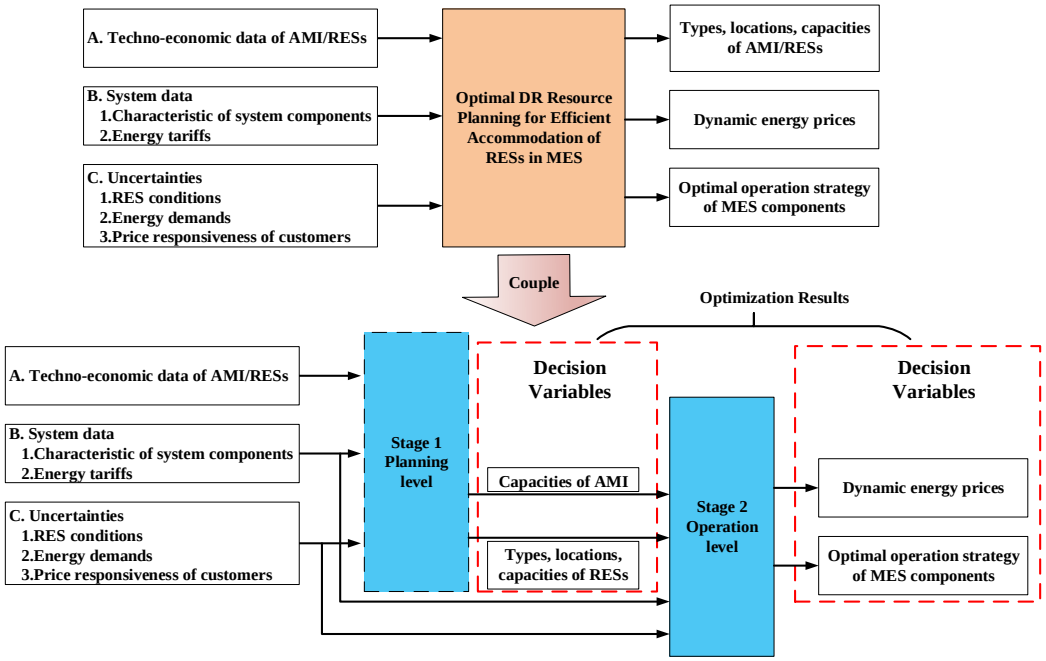

Fig. 2. Schematic Representation of the Proposed Planning Framework

The problem presented above is interpreted as a two-stage optimization model, as shown in Fig. 2. The proposed planning framework is decoupled into two stages: decision-making of MESO in the planning and operation phase. The first stage involves the determination of an optimal strategy for RESs and DR resource exploitation. The first-stage problem is to determine the types, locations and capacities of the RESs and AMI to be installed in the system, which make up the parameter set of the second-stage problem. In the second-stage optimization, the MESO combines RES conditions, forecasted energy demand, and price responsiveness of customers (own elasticities and cross elasticities) to optimize the strategy of RTP. The prices are designed to encourage system customers to adjust their demands so that the operation performance of MES can be optimized (i.e., the MESO's interests are maximized), subject to the constraints of the system components.

Note that the proposed model used to address the targeted problem corresponds to a centralized approach. Such a centralized approach tends to have good practical applicability in the current MES context, for the following reasons: 1) The proposed approach is mainly applicable for a centralized planning setting (which means all the decisions considered in the planning stages, such as the RES sizing and AMI placement, should be made by the same entity). In reality, such a setting is consistent with most of the distribution-level MES cases in China and other countries of the world. For example, in China, many distribution-level MES projects take the form of industrial parks. A private industrial park owner is in charge of both investment and operation issues of the MES. In this case, the proposed centralized approach

can be used as an efficient solution to the problem. 2) In contrast to the decentralized approach, the proposed approach is less complex and is the most straightforward way to achieve the optimal planning of MESs and ensure the global optimality of system performance. Therefore, it has good practical applicability in engineering. 3) In practice, the issue of computational complexity is regarded as one of the most significant factors hindering the adoption of the centralized approach. However, since the present study mainly focuses on a distribution-level MES (where the number of system buses (control objects) involved can be limited), this would help overcome the above bottleneck and gives the proposed approach favorable validity in real-world applications.

Solving the presented problem in Fig. 2 requires an accurate prediction of the system energy demands, customer price responsiveness, and expected production of RESs. However, in practice, accomplishing this tends to be extremely difficult for the MESO since these parameters can be stochastic in nature and may strongly correlate with each other in an unexpected way. To address this issue, a scenario-based stochastic programming modeling approach is employed in this study to address the uncertainties involved in our problem. By utilizing a series of correlation-handling techniques, a large number of discrete scenarios that represent the long-term statistical characteristics of the uncertain data can be generated. Considering that including all the scenarios (with correlated uncertainties) in an SP model could greatly increase the computational burden of the problem, a comprehensive scenario reduction method based on optimal clustering is further employed to eliminate the information redundancy in the resultant model and improve the computational efficiency of the problem.

3. Uncertainty Characterization

As mentioned above, in this study, the uncertainties associated with the MES come from the varying load demand, RES supply, and random price responsiveness of system customers. As such, this section details the mathematical models — probability density functions used to represent each of these uncertain variables in the proposed SP formulation.

A. Renewable energy sources

For the investigated MES, the generation of RESs is the first uncertain factor to be considered (Zeng et al., 2020a). In practice, although renewable power generation may take various forms (depending on the type of primary energy utilized), this work, for simplicity, explicitly discusses and focuses only on wind power as an illustrative example.

The power output of a wind turbine generator (WTG) mainly depends on the wind speed at the site. For long-term planning studies, the stochastic variability in wind speed v_t can usually be modelled by a two-parameter Weibull distribution (Karaki et al., 1999):

$$f(v_t;k,c)=\frac{k}{c}(\frac{v_t}{c})^{k-1}\exp\left[-\left(\frac{v_t}{c}\right)^k\right] \tag{1}$$

where k and c are the shape parameter and scale parameter, respectively.

Given the wind speed for a specific period v_t, the power output of a WTG can be approximated according to the characteristics of the wind turbine generation by the following function:

$$P^{WTG}(v_t)=\begin{cases}0, & 0\le v_t\le v^{in} \text{ or } v_t\ge v^{in}\\ \dfrac{(v_t-v^{in})P^{WTG-r}}{v^{ra}-v^{in}}, & v^{in}\le v_t\le v^{ra}\\ P^{\mathrm{WTG}-r}, & v^{ra}\le v_t\le v^{out}\end{cases} \tag{2}$$

where P^{WTG-r} denotes the rated active power of the installed WTG, and $v^{in}/v^{ra}/v^{out}$ are the cut-in, rated, and cut-out wind speeds, respectively.

To avoid excessive complexity, all WTG units in the discussed MES are assumed to be exposed to an identical wind regime and operate in the constant power factor mode during operation, which is consistent with (Zhang et al., 2018).

B. Energy demand

In an MES, the uncertainty of energy demand may arise from either the inherent volatility in customer consumption (Zhang et al., 2013) or load forecasting inaccuracy (Chen et al., 2019). According to the existing literature, the variation in different types of consumers' load demand over each time period can be roughly modeled by using a truncated Gaussian distribution, expressed as

$$f(D^0_{type,t})=\begin{cases}0, & D^0_{type,t}<D_{type,\min}\\ \dfrac{1}{\sqrt{2\pi}\sigma^D_{type,t}}\exp\left[-\dfrac{(D^0_{type,t}-\mu^D_{type,t})^2}{2(\sigma^D_{type,t})^2}\right], & D_{type,\min}\le D^0_{type,t}\le D_{type,\max}\\ 0, & D^0_{type,t}>D_{type,\max}\end{cases} \tag{3}$$

where $D^0_{type,t}$ denotes the random power/heat demand of different types of customers *type* in time-period *t*; $\mu^D_{type,t}$ and $\sigma^D_{type,t}$ are the statistical mean and standard deviation of the load demand for customer sector *type* in time period t, respectively; and $D_{type,\min}$ and $D_{type,\max}$ are the lower and upper bound values of the variation in $D^0_{type,t}$, respectively.

C. Demand-side responsiveness

In the RTP-based DR program, the demand responsivity of customers is defined by both the intrinsic operational characteristics of end-use loads (Zeng et al., 2021) and their sensitivity to price variations. According to (Zeng et al., 2019), the energy loads in an MES can generally be classified into three categories: critical loads (CLs), time-shiftable loads (TSLs), and energy-convertible loads (ECLs), in terms of the flexibility of their usage, and different mathematical models should be used to describe the DR capability associated with each type of the loads.

CLs are defined as the loads whose operation cannot be shifted or interrupted under any circumstances. Typical examples of CLs include refrigerators and cooking and lighting facilities. In practice, since most CL demands are related to the livelihood of individuals, these loads typically have no responsiveness to price signals and hence cannot be used for DR programs. As such, for a given time-period t, the energy demands of customers' CLs can be expressed as

$$D_t^{CL(\mathrm{e,h})} = D_t^{CL(\mathrm{e,h}),0} \tag{4}$$

where $D_t^{CL(e,h),0}$ represents the initial power/heat demand of CLs under the regular case (without DR).

TSLs are defined that energy demand can be flexibly settled within specified time periods as long as their total consumption remains constant. The most common TSLs are plug-in electric vehicles and water heaters. Unlike CLs, due to the temporally adjustable feature of their operation, TSLs can be exploited as an alternative resource for the DR program. In practice, if a change in energy price occurs in period t, the response of TSLs to this price variation as the modified demand can be described by (5), which is considered as the sum of consumers' reactions regarding the corresponding price change in the current period ($D_t^{TL(e,h),0}\left[1+\frac{\varepsilon_t^{TL(e,h)}\left(\rho_t^{(e,h)}-\rho_t^{(e,h),0}\right)}{\rho_t^{(e,h),0}}\right]$) plus that of other periods ($\sum_{t\prime\in T,t\prime\neq t} D_{t\prime}^{TL(e,h),0}\cdot \frac{\epsilon_{tt\prime}^{TL(e,h)}\left(\rho_{t\prime}^{(\mathrm{e,h})}-\rho_{t\prime}^{(e,h),0}\right)}{\rho_{t\prime}^{(e,h),0}}$).

$$D_t^{TL(\mathrm{e,h})} = D_t^{TL(\mathrm{e,h}),0}\left[1+\frac{\varepsilon_t^{TL(\mathrm{e,h})}\left(\rho_t^{(\mathrm{e,h})}-\rho_t^{(\mathrm{e,h}),0}\right)}{\rho_t^{(\mathrm{e,h}),0}}\right]+\sum_{t'\in T,t'\neq t} D_{t'}^{TL(\mathrm{e,h}),0}\cdot\frac{\epsilon_{tt'}^{TL(\mathrm{e,h})}\left(\rho_{t'}^{(\mathrm{e,h})}-\rho_{t'}^{(\mathrm{e,h}),0}\right)}{\rho_{t'}^{(\mathrm{e,h}),0}} \tag{5}$$

where $\rho_t^{(e,h)}$ and $\rho_t^{(e,h),0}$ denote the prices of energy sold to MES customers under the DR and regular case, respectively; $D_t^{TL(e,h)}$ and $D_t^{TL(e,h),0}$ are the corresponding energy demands of TSLs with respect to $\rho_t^{(e,h)}$ and $\rho_t^{(e,h),0}$, respectively; and $\varepsilon_t^{TL(e,h)}$ and $\epsilon_{tt\prime}^{TL(e,h)}$ are the own- and cross-price elasticity, respectively, reflecting the sensitivity of TSL consumption to the variation in relevant energy prices over

time. As such, the outcome of Eq. (5) is determined only by the operational characteristics of the concerned TSLs (i.e., the flexibility of the energy demand). In this study, for simplicity, the differences in TSL characteristics with respect to different group sectors are not distinguished, so all the parameters in Eq. (5) are general for all the consumers.

ECLs are defined as loads whose usage demand can be covered by different types of energy carriers. In practice, typical examples of ECLs may include industrial boilers, air conditioning equipment, and residential cooking appliances. Under a price-based DR program, the customers could be induced to switch the sources of the energy they use to satisfy the ECL demands, depending on the posted price of each energy carrier. For the two energy sources that constitute substitutes for each other (e.g., electricity and heat energy in this study), the expected demand of ECLs for a particular energy carrier under the RTP scheme can be described similarly as that of TSLs by using the elasticity-based model shown in (6)-(7). Specifically, Equation (6) is used to specify how the electricity-dependent demand of ECLs varies in response to the variation in electricity prices. Equation (7) represents the equality constraint of ECL consumption, which ensures that the total amount of energy consumed by the ECLs (i.e., the sum of energy inputs from different carriers) remains constant (Zeng et al., 2019).

$$D_t^{ELe} = D_t^{ELe,0}\left[1+\frac{\varepsilon_t^{EL}\left(\rho_t^{e}-\rho_t^{e,0}\right)}{\rho_t^{e,0}}\right]+\frac{D_t^{ELe,0}\epsilon_t^{EL}\left(\rho_t^{h}-\rho_t^{h,0}\right)}{\rho_t^{h,0}} \tag{6}$$

$$D_t^{ELh}-D_t^{ELh,0}=-\eta^{EL}\left(D_t^{ELe}-D_t^{ELe,0}\right) \tag{7}$$

where $D_t^{ELe}/D_t^{ELe,0}$ and $D_t^{ELh}/D_t^{ELh,0}$ denote the electricity and heat energy inputs of ECLs at period t under the DR/without DR, respectively; ρ_t^e/ρ_t^h and $\rho_t^{e,0}/\rho_t^{h,0}$ are the prices of electricity and heat under the DR and regular cases, respectively; η^{EL} is the efficiency of ECL energy utilization; and ε_t^{EL} and ϵ_t^{EL} are the own- and cross-elasticity coefficients, respectively, which indicate the sensitivity of ECL (electricity) demand to the corresponding real-time power and heat prices in period t.

For price-based DR programs, the demand-side responsiveness to price changes can be highly different depending on the idiosyncrasies of individuals (Zeng et al., 2014). As such, regarding the proposed DR model (4)-(7), the characteristic parameters (i.e., $\varepsilon_t^{TL(e,h)}$, $\epsilon_{tt'}^{TL(e,h)}$, ε_t^{EL} and ϵ_t^{EL}) in it tend to be uncertain for the MESO. In practice, the long-term statistical regularity in customers' demand behaviors can be learned by (Dagher, 2012). In this study, we assume that the uncertain price elasticity of MES users follows a uniform distribution that has upper and lower bounds equal to ±10% of the respective forecast values.

The corresponding probability density function can be expressed as:

$$f(z_t)=\begin{cases}1/(0.2\times\bar{z}_t), & 0.9\times\bar{z}_t < x < 1.1\times\bar{z}_t\\ 0, & \text{Otherwise}\end{cases} \tag{8}$$

where z_t is the symbol used to represent all the random elasticity parameters (i.e., $\varepsilon_t^{TL(e,h)}$, $\epsilon_{tt'}^{TL(e,h)}$, ε_t^{EL} and ϵ_t^{EL}) in this study; $\bar{z}_t$ denotes the corresponding forecast value of z_t.

4. Scenario Generation and Reduction

For the SP approach, given the probability density function of the uncertainties, the realization of these uncertainties in the optimization is represented by using a set of deterministic scenarios that may be generated based on various statistical simulation methods (Henrion and Römisch, 2018). A detailed description of the scenario generation and reduction procedure is presented below.

A. Modeling of correlations among uncertainties

In practice, two most widely used methods for describing the correlations among uncertainties are the Spearman correlation coefficient matrix and Pearson correlation coefficient matrix. Fundamentally distinct from the Pearson matrix (Press et al., 1992), the Spearman correlation coefficient matrix is capable of handling correlations among non-normally distributed random variables (Zhang et al., 2013). In our study, since it is assumed that the wind speed follows a Weibull distribution and the price elasticity of customers follows a uniform distribution, the Spearman matrix is a proper tool to be used for handling such correlations in this context.

According to (Zhang et al., 2013), the Spearman correlation coefficient matrix $\mathbb{C}_X$ of random variables $X_i\,(i=1,\ldots,n)$ can be expressed as

$$\mathbb{C}_X=\begin{bmatrix}1 & \kappa_{12} & \cdots & \kappa_{1n}\\ \kappa_{21} & 1 & \cdots & \kappa_{2n}\\ \vdots & \vdots & \ddots & \vdots\\ \kappa_{n1} & \kappa_{n2} & \cdots & 1\end{bmatrix} \tag{9}$$

where κ_{ij} denotes the Spearman correlation coefficient between random variables X_i and X_j, as derived by (10):

$$\kappa_{ij}=\frac{Cov\left(X_i,X_j\right)}{\sqrt{Var\left(X_i\right)}\sqrt{Var\left(X_j\right)}} \tag{10}$$

B. Scenario generation with correlated uncertainties

In this study, since both the wind speed and customers' demand elasticity follow non-normal probability

distributions, to generate the sample of these correlated uncertainties, the original distribution space first must be mapped to an independent standard normal distribution space. Then after this, the generation of the scenario for the correlated uncertain variables can be achieved by using Cholesky decomposition and the inverse transformation method (Qin et al., 2013a).

Let $X_i\,(i = 1, \ldots, n)$ denote the corresponding uncertain variables regarding wind speed, load demand and customers' price-elasticity and $\mathbb{C}_X$ represents the correlation matrix of these uncertainties, the main procedure for scenario generation can be summarized as follows:

(1) Based on the numerical search algorithm (Qin et al., 2013b), transform $\mathbb{C}_X$ into the corresponding standardized correlation matrix $\mathbb{C}_Y$, which has the variables $Y_i\,(i = 1, \ldots, n)$ consistent with a standard normal distribution.

(2) Generate a number of n-dimensional samples, where its elements follow a standard normal distribution and are independent of each other for every vector V.

(3) Apply the Cholesky decomposition technique to factorize matrix $\mathbb{C}_Y$ as $\mathbb{C}_Y = M_Y M_Y^T$ and produce the correlated normal distribution samples by following $Y = M_Y V$ (V is an n-dimensional vector comprising standard normally-distributed variables obtained from Step (2)), where the elements in Y are consistent with the correlation relationship represented by $\mathbb{C}_Y$.

(4) By using the inverse transformation $X_i = F_{X_i}^{-1}[\Phi(Y_i)](i = 1, \ldots, n)$ (where $\Phi(Y_i)$ is the standard normal cumulative distribution function of Y_i and $F_{X_i}^{-1}$ is the inverse function of the non-normal cumulative distribution function), the scenarios of correlated uncertainties $X_i\,(i = 1, \ldots, n)$ can be obtained from the resultant Y in Step (3).

C. Scenario reduction with correlated uncertainties

Since the computational burden of solving SP models heavily depends on the number of scenarios under concern, so a scenario reduction method should be applied to eliminate possible redundancies in the produced scenarios, so as to improve the solution efficiency of the problem, especially in large-scale systems.

In practice, the most commonly used scenario reduction methods basically aim to minimize the probability distance between the reserved scenario set and the original set (Heitsch and Römisch, 2003), and adopt this as the criterion of the scenario reduction (Henrion et al., 2009). However, in our study, since there are correlations among uncertainties, the resulting scenario set from the above probability-distance-based reduction methods may significantly deviate from the original dataset in terms of their statistical

properties, due to neglecting the potential impact of the correlation effect. As such, for the proposed SP model, to properly reduce the number of scenarios while maintaining the statistical correlations between uncertainties, a comprehensive scenario reduction method based on an optimal clustering framework is introduced in this study.

In contrast to the conventional probability-distance-based scenario reduction techniques, we develop an optimization model to determine the most representative scenarios from the original scenario set. The problem aims to maximize the sum of the probability similarity between the two sets in the statistical space while minimizing the sum of the degree of correlation loss after the scenario reduction, as mathematically described by (11):

$$\begin{aligned} &\max_{I_{\tilde{\tau}},\tilde{s}_{\tilde{\tau}}}\left[\sum_{\tilde{\tau}\in\tilde{\Omega}_1}\sum_{\tau\in I_{\tilde{\tau}}} Sim\left(s_\tau,\tilde{s}_{\tilde{\tau}}\right)-\beta\ corrloss\left(s_\tau,\tilde{s}_{\tilde{\tau}}\right)\right] \\ &s.t.\bigcup_{\tilde{\tau}\in\tilde{\Omega}_1} I_{\tilde{\tau}}=\Omega_1,\sum_{\tau\in\Omega_1} p_\tau=1, \\ &I_{\tilde{\tau}}\cap I_{\tilde{\tau}'}=\varnothing,\forall\,\tilde{\tau}\neq\tilde{\tau}',\tilde{\tau},\tilde{\tau}'\in\tilde{\Omega}_1 \end{aligned} \tag{11}$$

where Ω_1 is the original scenario set of size N_1 (represented by the original scenarios s_τ, corresponding probabilities p_τ, node $\tau \in \Omega_1$, and correlation coefficient matrix $\mathbb{C}_X$), and $\tilde{\Omega}_1$ is the reserved scenario set of size $\tilde{N}_1$ (represented by the preserved scenarios $\tilde{s}_{\tilde{\tau}}$, corresponding probabilities $\tilde{p}_{\tilde{\tau}}$, node $\tilde{\tau} \in \tilde{\Omega}_1$, and correlation coefficient matrix $\tilde{\mathbb{C}}_X$). $I_{\tilde{\tau}}$ denotes the clustering subset divided by τ, and node $\tilde{\tau}$ is then used to substitute the original nodes in subset $I_{\tilde{\tau}}$.

In (11), Sim is the function of probability similarity based on the traditional probability distance (Chen and Yan, 2018) and similarity function (Xie et al., 2010), which is used to indicate the statistical similarity degree between high-dimensional scenarios, as defined by (12). The larger Sim is, the greater the probability similarity is in the overall probability space.

$$\begin{aligned} &Sim\left(s_i,s_j\right) \\ &=\frac{1}{n}\left[\sum_{k=1}^{n}\left(1-\frac{p_i p_j}{p_i+p_j}\frac{\left|s_i^k-s_j^k\right|}{\left|\max\limits_{1\le l\le n}\left\{s_l^k\right\}-\min\limits_{1\le l\le n}\left\{s_l^k\right\}\right|+\varepsilon}\right)\right] \end{aligned} \tag{12}$$

where $k(k=1,2,\ldots,n)$ corresponds to the k-th random variable in the scenario vectors s_i (with probability p_i) and s_j (with probability p_j) in the *n*-dimensional scenario set of size N_1. ε is a small constant that prevents the numerator of the fraction from being divided by zero.

For (12), each random variable has the same effect in calculating Sim; as such, it prevents the issue that some random variables with larger dimensions play a major role to ensure the effectiveness of the

scenario reduction.

In addition, $corrloss$ in (11) refers to the correlation loss of uncertainties, which is based on the calculation of the Pearson correlation coefficient and is calculated as the sum of squares of the upper triangular elements in the correlation deviation matrix $\Delta\mathbb{C}_X$, as shown in (13)-(14).

$$\begin{aligned}\Delta\mathbb{C}_X &= \mathbb{C}_X - \tilde{\mathbb{C}}_X = \begin{bmatrix} 0 & \Delta\kappa_{12} & \cdots & \Delta\kappa_{1n} \\ \Delta\kappa_{21} & 0 & \cdots & \Delta\kappa_{2n} \\ \vdots & \vdots & \ddots & \vdots \\ \Delta\kappa_{n1} & \Delta\kappa_{n2} & \cdots & 0 \end{bmatrix} \\ &= \left(\Delta\kappa_{ij}\right)_{n\times n}, (i, j = 1, 2, ..., n)\end{aligned} \tag{13}$$

$$corrloss(s, \tilde{s}) = \sum_{i=1}^{n-1}\sum_{j=i+1}^{n}\left(\Delta\kappa_{ij}\right)^2 \tag{14}$$

The outcome of $corrloss$ reflects the degree of retention in the uncertainty correlation between the reduced scenarios $\tilde{s}(\tilde{s} \in \tilde{\Omega}_1)$ and the original scenarios $s(s \in \Omega_1)$. The smaller $corrloss(s, \tilde{s})$ is, the greater degree of retention meant to be achieved in the scenario reduction, which implies the better performance of the applied algorithm.

β in (11) is a weight coefficient. A smaller β is dedicated to selecting the reserved scenarios with higher statistical similarity but relatively greater loss of correlation effect after the reduction while a larger β guarantees a high degree of correlation preservation but lower similarity. Thus, by adjusting the value of β, a proper trade-off can be achieved in the scenario reduction between the two goals (Hu and Li, 2019).

The above-mentioned scenario reduction is implemented based on an iterative framework, and the description of the main steps is presented as follows:

(1) Compute the similarity matrix $SIM_{N_1\times N_1}$ with respect to each pair of original scenarios by $SIM(i, j) = Sim(s_i, s_j)$, according to (12).

(2) Calculate the correlation loss after deleting the selected s_i and s_j according to (14), and form $Corrloss_{N_1\times N_1}$ by following $Corrloss(i, j) = corrloss\left(s_{(s_i, s_j)}, \tilde{s}\right)$ (i.e., the refined scenarios without s_i and s_j in reference to the original ones $\tilde{s}$).

(3) Normalize the elements in matrices $SIM_{N_1\times N_1}$ and $Corrloss_{N_1\times N_1}$ based on (15) and (16) respectively and derive $SIM'_{N_1\times N_1}$ and $Corrloss'_{N_1\times N_1}$, as follows:

$$SIM'(i, j) = \frac{Sim(s_i, s_j) - SIM_{\min}}{SIM_{\max} - SIM_{\min}} \tag{15}$$

$$Corrloss'(i,j) = \frac{corrloss(s_i, s_j) - Corrloss_{\min}}{Corrloss_{\max} - Corrloss_{\min}} \tag{16}$$

(4) Form the total objective matrix $SIMCorr_{N_1 \times N_1}$ by $SIMCorr(i,j) = SIM'(i,j) - \beta Corrloss'(i,j)$.

(5) Determine the optimal scenario pair (s_i, s_j) corresponding to the maximum value in $SIMCorr_{N_1 \times N_1}$ by solving (11).

(6) Combine the two selected scenarios (s_i, s_j) into a single one s_{new} with the corresponding probability p_{new} according to the "optimal redistribution rule" (Dupačová et al., 2003), as shown in (17) and (18):

$$s_{new} = \frac{p_i s_i + p_j s_j}{p_i + p_j} \tag{17}$$

$$p_{new} = p_i + p_j \tag{18}$$

(7) Substitute (s_i, s_j) with s_{new} to form the refined scenario set $\tilde{\Omega}_1$. Accordingly, the number of remaining scenarios N_1 decreases by one.

(8) Check whether the size of $\tilde{\Omega}_1$ is equal to the predetermined value $\tilde{N}_1$. If yes, export the derived $\tilde{\Omega}_1$, and terminate the procedure; otherwise, go back to Step (1) and continue.

Through the above procedures, a refined scenario set $\tilde{\Omega}_1$ can be obtained wherein the redundant scenarios with similar statistical properties in the initial scenario set are excluded while considering the correlations among uncertainties. As such, the proposed SP problem can be solved more efficiently while fully maintaining the character of the original system.

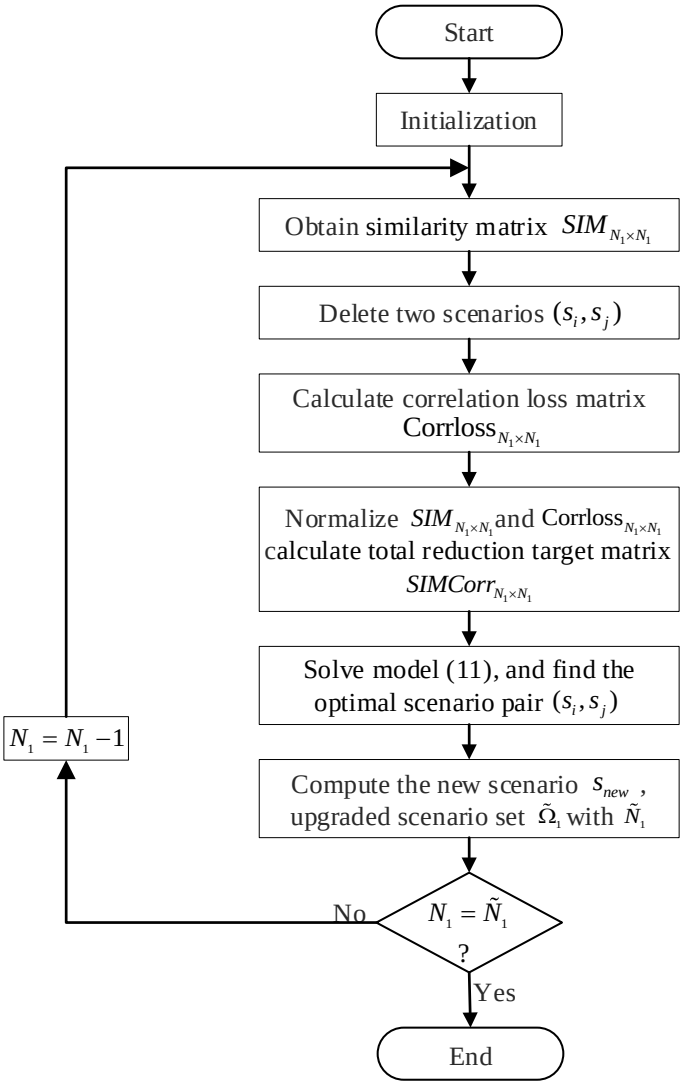

Fig. 3. Flowchart of Scenario Reduction

5. Mathematical Formulation

The formulation of the proposed MES planning problem can be presented as Eqs. (19)-(32e).

$$\min\left(OF + OS\right) \tag{19}$$

where

$$OF = IC + MC \tag{20}$$

$$IC = \sum_{w \in \Omega_w} \tau^{WTG} cc^{WTG} n_w + \sum_{d \in \Omega_d} \tau^{AMI} cc^{AMI} N_d^{household} \chi_d \tag{21a}$$

$$MC = \sum_{w \in \Omega_w} cm^{WTG} n_w + \sum_{d \in \Omega_d} cm^{AMI} N_d^{household} \chi_d + cm^{Trans} P^{Trans-r} + cm^{CHP} P^{CHP-r} \tag{21b}$$

subject to

$$0 \le n_w \le n_w^{\max} \quad \forall w \in \Omega_w \tag{22a}$$

$$0 \le \chi_d \le 1 \quad \forall d \in \Omega_d \tag{22b}$$

with

$$OS = EP + RE \tag{23}$$

$$EP = \theta \sum_{s \in \Omega_s} p_s \bullet \left[\sum_{t \in T} (\sigma_t^{GR} P_{s,t}^{GR} + \sigma_t^{GS} G_{s,t}^{GS}) \right] \tag{24a}$$

$$RE = \theta \sum_{s \in \Omega_s} p_s \bullet \left\{ \begin{array}{c} \sum_{d \in \Omega_d} \sum_{t \in T} \left[\left(\rho_{s,d,t}^{e,0} PD_{s,d,t}^{TL,0} - \rho_{s,d,t}^{e} PD_{s,d,t}^{TL} \right) + \left(\rho_{s,d,t}^{e,0} PD_{s,d,t}^{EL,0} - \rho_{s,d,t}^{e} PD_{s,d,t}^{EL} \right) \right. \\ \left. + \left(\rho_{s,d,t}^{h,0} HD_{s,d,t}^{EL,0} - \rho_{s,d,t}^{h} HD_{s,d,t}^{EL} \right) \right] \end{array} \right\} \tag{24b}$$

subject to

$$P_{s,t}^{GR} = \sum_{i \in \Omega_I} P_{s,i,t}^{Trans} \qquad \forall s \in \Omega_s, \forall i \in \Omega_I, \forall t \in T \tag{25a}$$

$$G_{s,t}^{GS} = \sum_{i \in \Omega_I} G_{s,i,t}^{CHP} \qquad \forall s \in \Omega_s, \forall i \in \Omega_I, \forall t \in T \tag{25b}$$

$$0 \le P_{s,t}^{GR} \le P^{GR\max} \quad \forall s \in \Omega_s, \forall t \in T \tag{26a}$$

$$0 \le G_{s,t}^{GS} \le G^{GS\max} \quad \forall s \in \Omega_s, \forall t \in T \tag{26b}$$

$$\rho_{s,d,t}^{e,0} \lambda_{\min} \le \rho_{s,d,t}^{e} \le \rho_{s,d,t}^{e,0} \lambda_{\max} \quad \forall s \in \Omega_s, \forall d \in \Omega_d, \forall t \in T \tag{27a}$$

$$\rho_{s,d,t}^{h,0} \lambda_{\min} \le \rho_{s,d,t}^{h} \le \rho_{s,d,t}^{h,0} \lambda_{\max} \quad \forall s \in \Omega_s, \forall d \in \Omega_d, \forall t \in T \tag{27b}$$

$$P_{s,i,t}^{CHP} = \gamma \times H_{s,i,t}^{CHP} \quad \forall s \in \Omega_s, \forall i \in \Omega_I, \forall t \in T \tag{28a}$$

$$G_{s,i,t}^{CHP} = H_{s,i,t}^{CHP} \big/ (HV \times \eta^{CHP}) \quad \forall s \in \Omega_s, \forall i \in \Omega_I, \forall t \in T \tag{28b}$$

$$0 \le P_{s,i,t}^{CHP} \le P_i^{CHP-r} \quad \forall s \in \Omega_s, \forall i \in \Omega_I, \forall t \in T \tag{29a}$$

$$0 \le P_{s,i,t}^{Trans} \le P_i^{Trans-r} \quad \forall s \in \Omega_s, \forall i \in \Omega_I, \forall t \in T \tag{29b}$$

$$0 \le P_{s,i,t}^{WTG} \le n_i P_i^{WTG-r} \quad \forall s \in \Omega_s, \forall i \in \Omega_I, \forall t \in T \tag{29c}$$

$$\begin{array}{l} P_{s,i,t}^{CHP} + P_{s,i,t}^{Trans} + P_{s,i,t}^{WTG} - \sum_{\substack{i,j \in \Omega_I \\ j \ne i}} P_{s,ij,t} \\ = (1\text{-}\chi_i)(PD_{s,i,t}^{CL,0} + PD_{s,i,t}^{TL,0} + PD_{s,i,t}^{EL,0}) + \chi_i (PD_{s,i,t}^{CL} + PD_{s,i,t}^{TL} + PD_{s,i,t}^{EL}) \\ \forall s \in \Omega_s, \forall i, j \in \Omega_I, \forall t \in T \end{array} \tag{30a}$$

$$\begin{aligned}&Q_{s,i,t}^{CHP}+Q_{s,i,t}^{Trans}+Q_{s,i,t}^{WTG}-\sum_{\substack{i,j\in\Omega_I\\ j\neq i}}Q_{s,ij,t}\\&=(1-\chi_i)(QD_{s,i,t}^{CL,0}+QD_{s,i,t}^{TL,0}+QD_{s,i,t}^{EL,0})+\chi_i(QD_{s,i,t}^{CL}+QD_{s,i,t}^{TL}+QD_{s,i,t}^{EL})\\&\forall s\in\Omega_s,\forall i,j\in\Omega_I,\forall t\in T\end{aligned}\tag{30b}$$

$$\begin{aligned}&H_{s,i,t}^{CHP}-\sum_{\substack{i,j\in\Omega_I\\ j\neq i}}H_{s,ij,t}=\\&(1-\chi_i)(HD_{s,i,t}^{CL,0}+HD_{s,i,t}^{TL,0}+PD_{s,i,t}^{EL,0})+\chi_i(HD_{s,i,t}^{CL}+HD_{s,i,t}^{TL}+HD_{s,i,t}^{EL})\\&\forall s\in\Omega_s,\forall i,j\in\Omega_I,\forall t\in T\end{aligned}\tag{30c}$$

$$\begin{aligned}&\begin{cases}P_{s,i+1,t}=P_{s,i,t}-PD_{s,i+1,t}\\Q_{s,i+1,t}=Q_{s,i,t}-QD_{s,i+1,t}\\V_{s,i+1,t}=V_{s,i,t}-2\dfrac{r_iP_{s,i,t}+x_iQ_{s,i,t}}{V_0}\end{cases}\\&\forall s\in\Omega_s,\forall i,j\in\Omega_I,\forall t\in T\end{aligned}\tag{31a}$$

$$\begin{aligned}&\begin{cases}H_{s,ij,t}^{'}=-H_{s,ji,t}^{'}+\Delta H_{s,ij,t}^{'}\\\Delta H_{s,ij,t}^{'}=2\pi\dfrac{TE^{sw}-TE^{e}}{\sum R}l_{ij}\end{cases}\\&\forall s\in\Omega_s,\forall i,j\in\Omega_I,\forall t\in T\end{aligned}\tag{31b}$$

$$V_i^{\min}\le V_{s,t}\le V_i^{\max}\quad\forall s\in\Omega_s,\forall i\in\Omega_I,\forall t\in T\tag{32a}$$

$$0\le I_{s,ij,t}\le I_{ij}^{\max}\quad if\ I_{s,ij,t}\ge 0\quad\forall s\in\Omega_s,\forall i,j\in\Omega_I,\forall t\in T\tag{32b}$$

$$P_{ij}^{\min}\le P_{s,ij,t}\le P_{ij}^{\max}\quad if\ P_{s,ij,t}\ge 0\quad\forall s\in\Omega_s,\forall i,j\in\Omega_I,\forall t\in T\tag{32c}$$

$$Q_{ij}^{\min}\le Q_{s,ij,t}\le Q_{ij}^{\max}\quad if\ Q_{s,ij,t}\ge 0\quad\forall s\in\Omega_s,\forall i,j\in\Omega_I,\forall t\in T\tag{32d}$$

$$H_{ij}^{'\min}\le H_{s,ij,t}^{'}\le H_{ij}^{'\max}\quad if\ H_{s,ij,t}^{'}\ge 0\quad\forall s\in\Omega_s,\forall i,j\in\Omega_I,\forall t\in T\tag{32e}$$

As shown in (19), the objective of the proposed model is to minimize the total annualized cost of the system, which is the sum of the corresponding costs occurred in the planning stage (OF) and the operation stage (OS). Specifically, the total payment associated with the planning stage (OF) comprises by the system investment cost (IC) and maintenance cost (MC). The investment cost (IC) involves the capital cost of MES components (i.e., renewable energy generation and AMI units and is determined by the installed capacity of each type of equipment. An annualization factor τ is used to convert equipment values into comparable quantities on an annual basis, as shown in (21a). The maintenance cost (MC) is incurred by the routine inspection of the system, which is calculated as the product of the related annual cost and the size with respect to each type of deployed component, as presented in (21b). On the other hand, the total payment pertaining to the operation phase (OS) comprises the system energy procurement cost (EP) and DR cost

(RE), as shown in (23). The energy procurement cost (EP) is incurred by the MES purchasing electricity and natural gas from external energy market and is computed as the product of market price and the corresponding quantity of energy that the MES purchases, as shown in (24a). For DR cost (RE), it is incurred by the implementation of the DR program. It is computed as the difference between the MES owner's revenue in the DR scenario and that for the regular case, as represented in (24b). The obtained system energy procurement cost (EP) and DR cost (RE) are summed and aggregated over the considered scenario set (allowing for the probability of occurrence of each scenario) to derive the overall expected operation cost of the system under the realization of uncertainties.

For the first-stage optimization, constraint (22a) imposes the limits for the maximum and minimum capacity of RES generation units that could be installed in the MES. Besides, as a household can be equipped with no more than one AMI unit, the penetration rate of AMI is limited to 100%, as confirmed by (22b). For the second-stage constraints, balances of supply and demand are confirmed by Eq. (25a)-Eq. (25b), and Eq. (26a) and (26b) are used to confirm that the power/gas procured from the external market must not exceed the available capacity, and reverse power flow is forbidden. Eqs. (27a) and (27b) stipulate that the offered tariff by MESO can be higher than the market acquisition price but cannot exceed a predefined "cap" value. Furthermore, the operation constraints of CHP units are represented by Eq. (28a)-(28b), considering their power-thermal coupling characteristics. Constraints (29a)-(29c) present the potential power output of CHP units, transformers and wind turbines. The conventional equality constraints for the gas flow, power flow and heat flow in the system are represented by Eq. (30a)-(30c). Eq. (31a) and (31b) represent the linearized power flow and linear thermal energy flow equations, which have been extensively used in the MES analysis (Gu et al., 2017). The operation bounds of power network and the heat network are represented by Eq. (32a)-(32e).

The decision variables for the first-stage problem encompass the optimal types, locations and capacities of the RESs and AMI to be installed, i.e., $\{w, n_w, d, \chi_d\}$, and these make up the parameter set of the second-stage optimization. The decision variables for the second-stage model include the optimal design of the price tariff $\{\rho^e_{s,d,t}, \rho^h_{s,d,t}\}$; the operational status of CHP units, transformers and wind turbines $\{P^{CHP}_{s,i,t}, P^{Trans}_{s,i,t}, P^{WTG}_{s,i,t}\}$; and the amount of electricity/gas procured from a local grid/gas station $\{P^{GR}_{s,t}, G^{GS}_{s,t}\}$ in each scenario and the time block of the planning horizon.

Mathematically, the proposed model in (19)-(32e) is a typical mixed-integer quadratic programming problem that is readily solvable by using various commercial solvers.

6. Case Study

A. Test system and data

To illustrate the effectiveness of the model proposed in this paper, a series of numerical studies are conducted based on a combined electricity-thermal system extracted from (Liu et al., 2016). The concerned test system comprises a 32-node low-temperature district heating network and a nine-node distribution power network, which are coupled by three CHP units. The topological diagram of the system is shown in Fig. 4.

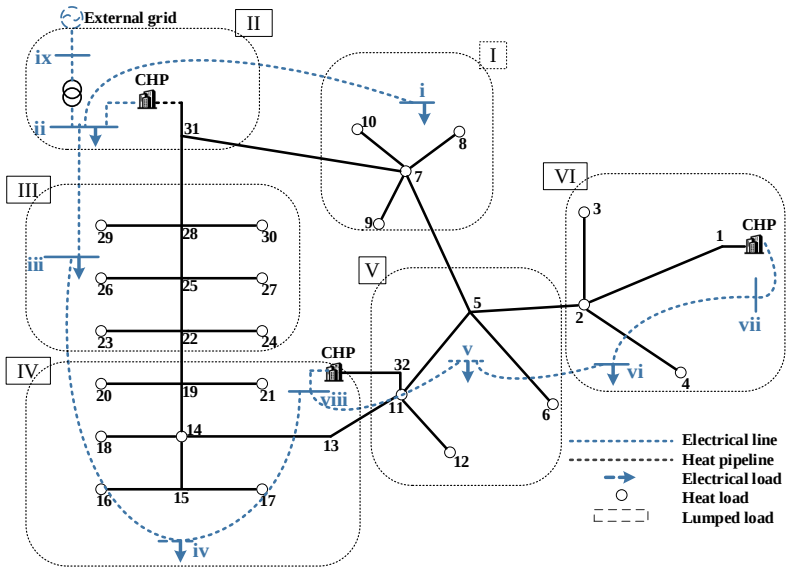

Fig. 4. Topological Diagram of Test System

As seen, the concerned MES is divided into six segments. Each segment is considered one aggregator that may respond to the RTP offered by the MESO on behalf of all the corresponding customers in the area.

To ensure the applicable of the proposed planning scheme in practical situations, we use a four-day equivalent model to represent the seasonal variation in customer load demand over a full year, as shown in Fig. 5. Each day in the presented four-day model has a distinctive average load profile, which represents the median (typical value) of the three consecutive months that compose a season (spring, summer, fall, and winter). The information about the load demand for each segment is provided in Table 2. In this study, a truncated Gaussian distribution is used to describe the uncertainty of customer energy demands in (3), which has a mean equal to their forecasted value and a variance of unity.

Table 2 Average Values of System Load Demands (kW)

System segment	I	II	III	IV	V	VI

Customer type	Residential	NAN	Industrial	Industrial	Residential	Commercial
Electrical demand	200	0	700	700	200	400
Heat demand	333	0	780	1177	360	667

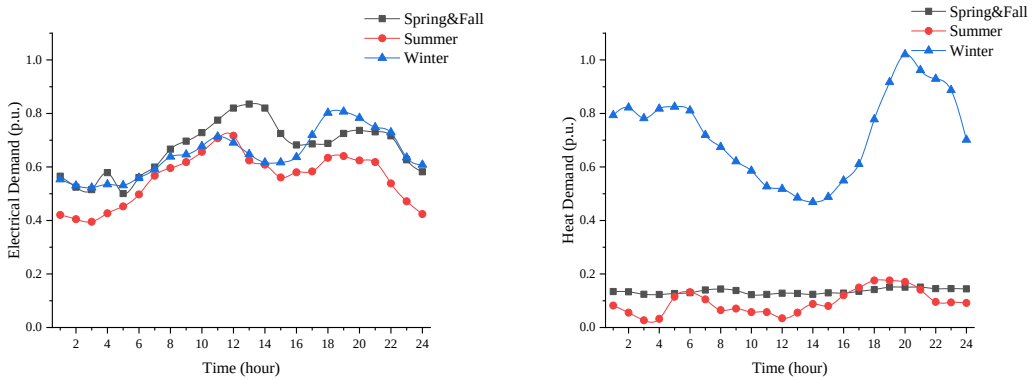

Fig. 5. Electrical and Heat Demand Profiles in Different Seasons

The load composition of customers in each season is shown in Table 3, which is based on metered consumption records from a demonstration MES project in Beijing and show the diversity of the load composition for different types of customers. In addition, the price elasticity values applied to customers' TSLs/ECLs are shown in Table 4. The own-price elasticities are determined based on real socio-economic surveys by (Labandeira et al., 2017), and the cross-price elasticity data is extracted from (Woo et al., 2018). In this study, since each customer sector is assumed to have a distinct load composition and consumption pattern, their elasticity values differ accordingly.

Table 3 Seasonal Variation of System Load Demand (p.u.)

Season	Customer sector	$D_t^{CLe,0}$	$D_t^{TSLe,0}$	$D_t^{ESLe,0}$	$D_t^{CLh,0}$	$D_t^{ESLh,0}$
Spring	Residential	0.15	0.4	0.45	0.55	0.45
&	Commercial	0.5	0.2	0.3	0.7	0.3
Fall	Industrial	0.7	0.1	0.2	0.8	0.2
	Residential	0.3	0.4	0.3	0.7	0.3
Summer	Commercial	0.7	0.2	0.1	0.9	0.1
	Industrial	0.8	0.1	0.1	0.9	0.1
	Residential	0.2	0.4	0.4	0.7	0.3
Winter	Commercial	0.6	0.2	0.2	0.8	0.2
	Industrial	0.8	0.1	0.1	0.9	0.1

Table 4 Price Elasticity of TSLs/ECLs

Time period	ε_t^{TLe}	$\epsilon_{tt'}^{TLe}$	ε_t^{EL}	ϵ_t^{EL}
22:00-7:00	-0.33	0.02	-0.33	0.92
7:00-8:00; 11:00-18:00	-0.45	0.02	-0.45	0.99
8:00-11:00; 18:00-22:00	-0.62	0.03	-0.62	1.21

In the concerned test case, it is assumed that the candidate sites for WTG/AMI installation are Bus-i at Segment-I, Bus-iv at Segment-IV and Bus-vi at Segment-VI. The maximum allowed WTG capacity is set to 500 kW for each bus. Table 5 reports the parameter settings in our simulation; the parameters of WTG are determined according to (Zhang et al., 2018), and the parameters of AMI are from (Luan, 2009). We assume that all parameters are constant during the planning horizon. Additionally, the discount rate is set to 6%.

Table 5 Parameter Settings

	Parameter value	
	Technical	Cost
WTG	P^{WTG-r}=100 kW	
	v_{in}^{c}=3 m/s	cc^{WT}=1114 \$/kW
	v_{out}^{c}=17 m/s	cm^{WT}=21 \$/kW
	ζ^{WT}=20 years	
AMI	ζ^{es}=20 years	cc^{AMI}=90 \$/unit
		cm^{AMI}=1.65 \$/unit

The uncertainty of wind speed is described by using a Weibull distribution in (1). The shape parameter and scale parameter of the Weibull distribution are obtained by fitting the real wind speed statistics from 2013-2015 collected in Beijing and reported in Table 6.

Table 6 Parameter Value of Wind Speed Distribution

Season	Parameter	22:00-7:00	7:00-8:00; 11:00-18:00	8:00-11:00; 18:00-22:00
Spring	c	9.47	9.01	8.67
	k	4.06	4.21	4.52
Summer	c	5.41	4.91	4.88
	k	2.38	2.41	2.45
Fall	c	7.98	7.33	6.82
	k	4.11	4.23	4.56
Winter	c	9.47	9.03	8.65
	k	3.97	4.23	4.25

In addition, the correlation coefficients among different uncertainties (i.e., RES generation, load demand and demand price elasticity) in this study are shown in Table 7 and are determined according to statistical survey data of Beijing.

Table 7 Correlation Matrices of Uncertainties

Time period	$\mathbb{C}_X$
22:00-7:00	$\begin{bmatrix} 1.00 & 0.24 & 0.08 \\ 0.24 & 1.00 & 0.74 \\ 0.08 & 0.74 & 1.00 \end{bmatrix}$

7:00-8:00; 11:00-18:00	$\begin{bmatrix} 1.00 & 0.42 & 0.11 \\ 0.42 & 1.00 & 0.78 \\ 0.11 & 0.78 & 1.00 \end{bmatrix}$
8:00-11:00; 18:00-22:00	$\begin{bmatrix} 1.00 & 0.44 & 0.11 \\ 0.44 & 1.00 & 0.78 \\ 0.11 & 0.78 & 1.00 \end{bmatrix}$

The hourly power acquisition price of the MESO is shown in Fig. 6, which is based on the real tariff from Hunan Province, China. The gas procurement price is set to a constant value of 0.143 \$/m^3. In the regular case (without DR), the prices for customers to procure electricity and heat from the MES are set to 0.114 \$/kWh and 0.043 \$/kWh, respectively (Gu et al., 2017). The upper limit of the imposed RTP ($\delta_{d,t}^{ch}$) is set to 150% of the corresponding energy acquisition price in each time period t, i.e., $\rho_{\max}^{e} = 1.5 \times \sigma_t^{GR}$.

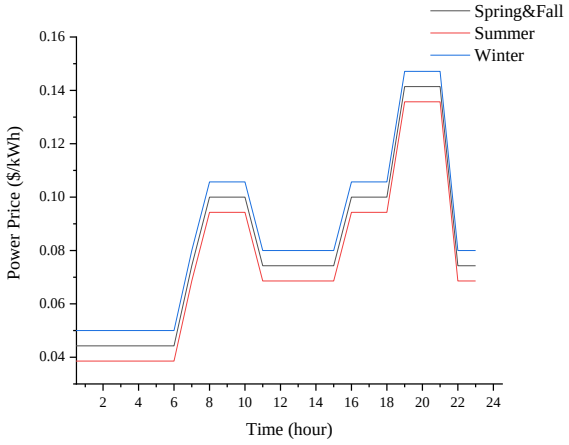

Fig. 6. Hourly Electricity Price from the External Market for Different Seasons

The proposed mixed-integer quadratic programming problem is programmed in the Matlab environment and is solved using the Yalmip with default settings. The model is implemented on a desktop computer with an Intel Core Duo 2.2 GHz processor and 4 GB of RAM.

B. Results

In this study, DR is considered as a strategic flexibility resource and is utilized to improve the efficiency of RES exploitation in an MES planning context. To illustrate the effectiveness of the proposed planning approach and its added value to the state-of-the-art solutions, a comparative analysis is conducted in this section, considering methods found in the literature.

For this aim, three cases are defined and considered for the purpose of comparison, which are named Benchmark, C1 and C2, respectively. Specifically, the Benchmark scenario represents the MES case without WTGs or DR. This case is used as the reference for indicating how the performance of MES changes with different planning schemes adopted. For C1, we assume that the load demands of the system customers are inelastic and nonresponsive to the variation in energy prices. In other words, in this case, the

MES planning is performed without considering the DR option. It represents the conventional approach for renewable energy generation planning that extensively discussed in the existing literature, such as (Mehrjerdi, 2020). Finally, for C2, we consider that the electricity and heat demands are elastic and price-dependent. In other words, the proposed integrated planning model for WTG and DR is considered in this case.

Table 8 gives the optimization results of the study, and an evaluation of the obtained planning schemes is tabulated in Table 9.

Table 8 Optimal Planning Schemes for Different Cases

System segment	I	IV	VI
Benchmark	N/A	N/A	N/A
C1	WTG-100 kW (Bus-i)	WTG-200 kW (Bus-iv)	WTG-100 kW (Bus-vi)
C2	WTG-100 kW (Bus-i) AMI-100% (Segment-I)	WTG-200 kW (Bus-iv) AMI-100% (Segment-IV)	WTG-100 kW (Bus-vi) AMI-100% (Segment-VI)

Table 9 Evaluation of Obtained Planning Schemes (k$)

System segment		I	II	III	IV	V	VI	Total
Benchmark	IC	0.00	0.00	0.00	0.00	0.00	0.00	0.00
	MC	0.00	8.14	0.00	27.00	0.00	11.57	46.71
	EP	188.69	0.00	611.39	660.41	191.97	377.38	2029.83
	RE	0.00	0.00	0.00	0.00	0.00	0.00	0.00
	Total cost							2076.54
C1	IC	9.71	0.00	0.00	19.43	0.00	9.71	38.86
	MC	2.14	8.14	0.00	31.29	0.00	13.71	55.29
	EP	170.74	0.00	611.39	597.58	191.97	341.47	1913.14
	RE	0.00	0.00	0.00	0.00	0.00	0.00	0.00
	Total cost							2007.29
C2	IC	10.11	0.00	0.00	19.82	0.00	10.11	40.04
	MC	2.23	0.81	0.00	31.37	0.00	13.80	48.21
	EP	148.41	0.00	611.39	585.49	191.97	321.53	1858.79
	RE	12.47	0.00	0.00	-87.50	0.00	-19.39	-94.42
	Total cost							1852.62

*The annualized investment cost of the system (IC), annual maintenance cost (MC), energy procurement cost (EP), and potential loss of revenue (RE)

(1) Economic Benefits

The optimization results of the three cases are compared in Table 8. Compared with the Benchmark

case, regardless of whether DR is included or not, the total cost of the system is greatly reduced by the allocation of renewable generation units. Moreover, the economic costs associated with C2 are far less than those associated with C1, which implies that the implementation of DR indeed brings about significant benefits to the system.

More specifically, with the implementation of only WTG allocation, the cost of energy procurement and the total system cost decrease by 6.0% and 3.3%, respectively, compared with the Benchmark case. It is clear that since wind power generation replaces part of the electricity imported from the market, this helps to reduce the operating cost of the system, and such a decrease also offsets the investment cost of WTGs.

Considering both WTGs and DR, the WTG allocation scheme in C2 is the same as that in C1, and the penetration ratio of AMI of all candidate buses in C2 is 100%. These results show that the flexibility of customer demands is used as an additional balancing resource for mitigating the intermittency of wind power generation and promoting the exploitation of renewable energy resources in C2. The cost of energy procurement in C2 decreases by 2.84% and 8.43% compared with C1 and the Benchmark case, respectively. Moreover, after calculation, the revenue increases by 94.42 (k$) per year in C2. These increased economic benefits are conducive to encouraging the implementation of the DR program.

(2) Renewable Energy Utilization

To reveal the contribution that DR makes to the utilization of RES, Figures 7 to 10 further illustrate the power balance of the system and the demand changes under C1 and C2 for a typical day at Segment-I. Specifically, Fig. 7 shows the energy scheduling of each MES component with and without consideration of DR; Figs. 8 and 9 show the imposed tariff and the corresponding system load demand changes after introducing DR. Finally, the wind power generation in the two cases is compared and displayed in Fig. 10.

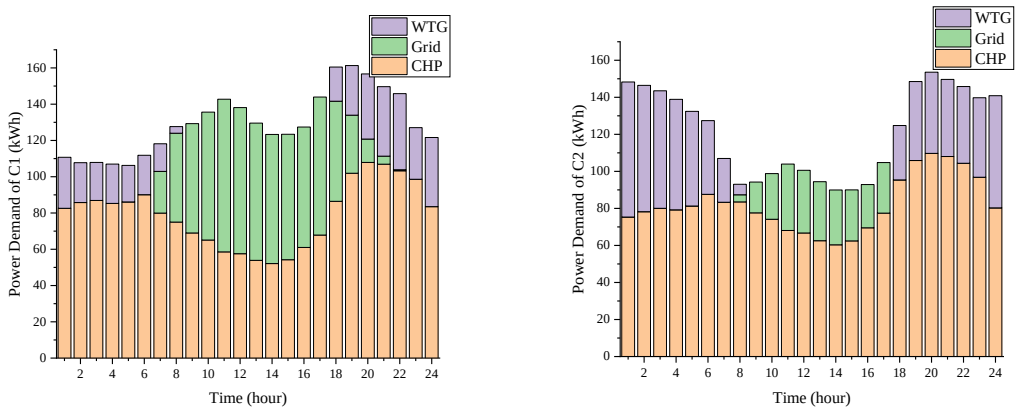

Fig. 7. Electric Power Balance of System Segment-I in C1 and C2

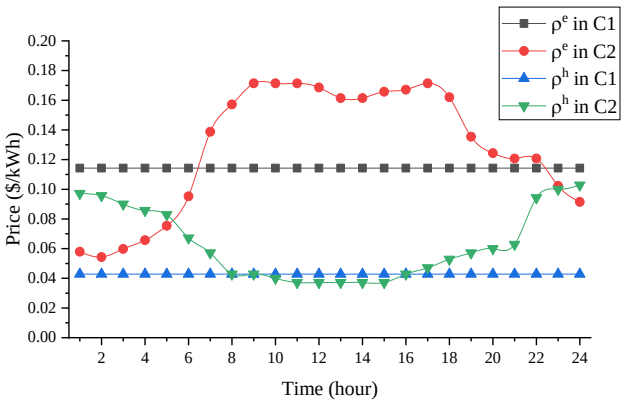

Fig. 8. Energy Tariff Offered to Customers

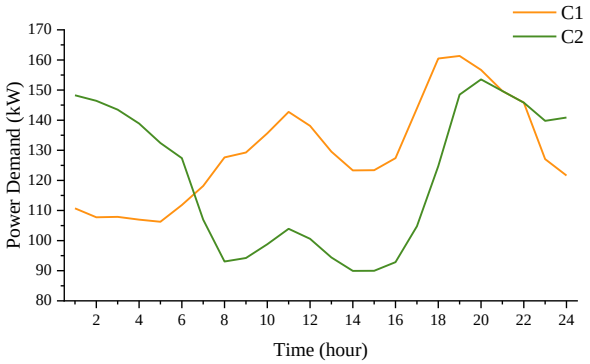

a) Power Load Demand

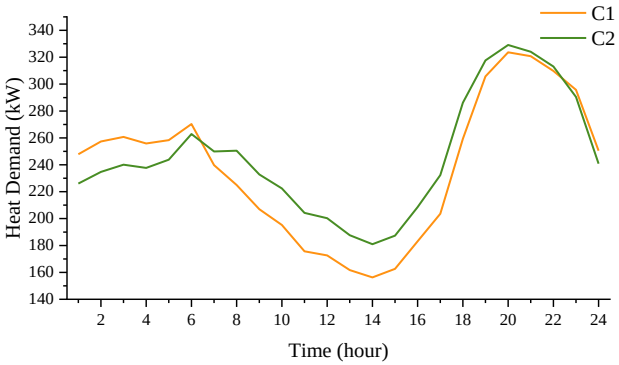

b) Heat Load Demand

Fig. 9. Comparison of System Load Demand in C1 and C2

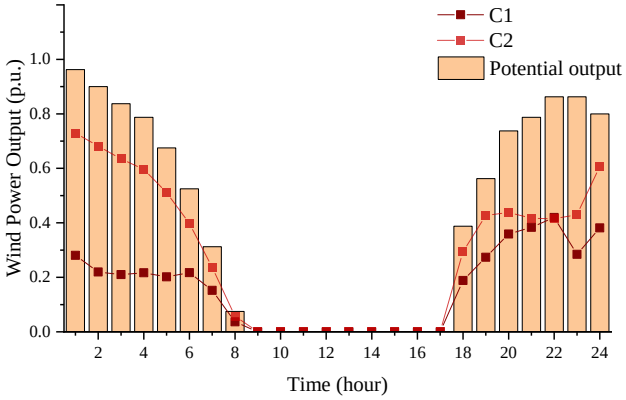

Fig. 10. Comparison of Wind Power Generation in C1 and C2

After DR is implemented, Fig. 8 shows that the electricity price and heat price change significantly in each time period. The peak electricity price period mainly occurs from 10:00 to 18:00, while low electricity prices are mainly concentrated from 22:00 to 6:00. For the heat prices, the trend is the opposite. Due to the RTP mechanism, the load demand can be flexibly adjusted according to the operational state of the system, and there is consistency between the user's overall daily electricity load curve and the RES output, as shown in Fig. 9.

It can be observed from Fig. 10 that wind power curtailment occurs only during off-peak hours of electricity loads. To meet the user's heat demand, CHP units must be dispatched to generate a certain amount of electricity, which reduces the output of wind power generation. However, after DR is introduced, wind power curtailment can be significantly alleviated due to the flexibility of the load demand. During off-peak hours, relatively low electricity prices cause consumers to shift their heating demand to electric heating, resulting in reductions in power generation from CHP and electricity imported from the external market; thus, the utilization of wind power increases accordingly. The curtailment rate of wind power decreases by 9.4%. In other words, the wind power utilization rate increases to 71.1%, which is much higher than that without DR.

C. Further discussions

(1) Comparison with Existing Works

To justify the novelty of the proposed planning method and its advantages over existing studies, a further comparative analysis is conducted in this section. Considering the large amount of existing literatures in this research field, to facilitate this comparison, we divide all the literatures presented in Table 1 into three categories (which are named as “Group-1”, “Group-2”, and “Group-3”), according to the salient feature they have in common. As shown in Table 10, specifically, in Group-1, all the literatures involved

feature in that they all failed to take account of DR potential in the system planning. In Group-2, all the literatures involved feature in that they all resorted to a deterministic modeling approach to describe the effect of DR (i.e., neglecting the potential random nature of DR in the system operation), instead of using a stochastic modeling approach. As for Group-3, all the literatures involved feature in that they all account for the impact of uncertainties in the system planning, but all of them failed to consider the potential correlations among different uncertain factors.

In contrast to any existing studies in Group-1, Group-2 or Group-3, this paper proposes a new MES planning framework which comprehensively considers the issues including the stochastic nature of DR, the synergy between DR and RES, and the potential correlations among uncertainties, in the decision-making. We compare the optimal planning results derived by using the proposed method and the corresponding methods in Group-1, Group-2, and Group-3. The calculation results are presented in Table 11.

Table 10 Classification of Existing Literatures in Table 1

Method	Feature			References in Table 1
	DR	Uncertainty modeling	Correlation	
Group-1	×	×	×	(L. Gan et al., 2016), (Jangamshetti and Rau, 2001) (Qadrdan et al., 2017), (Zhang et al., 2020), (Eissa, 2019), (Pan et al., 2019),
Group-2	√	×	×	(Bahrami and Sheikhi, 2016), (Sheikhi et al., 2015), (Rastegar et al., 2015), (Liu et al., 2018b), (Shao et al., 2018), (Liu et al., 2018a), (Sheikhi et al., 2016)
Group-3	√	√	×	(Mehrjerdi and Hemmati, 2020), (Zhang et al., 2016a), (Pazouki and Haghifam, 2016), (Zhang et al., 2016b), (Kim and Norford, 2017), (Dolatabadi and Mohammadi-Ivatloo, 2017), (Neyestani et al., 2015)
Proposed	√	√	√	-

Table 11 Optimization Results Based on Different Uncertainty Modeling Approaches (k$)

Method	IC	MC	EP	RE	Objective	Regret value
Group-1	38.86	55.29	1913.14	-	2007.29	14.18
Group-2	30.31	46.00	1840.75	-95.13	1821.93	13.29
Group-3	40.04	48.21	1878.89	-99.91	1867.23	3.96
Proposed	40.04	48.21	1858.79	-94.42	1852.62	1.54

To give an insight into the above calculations, we first focus on the result comparison between Group-1 and the proposed case. As can be seen, when the DR program is excluded (as represented by the case in Group-1), the optimal planning solution corresponds to a total cost of 2007.29 k$, which is much higher than the outcome with inclusion of DR (1852.62 k$). This demonstrates that the proper utilization of DR program can indeed bring about significant benefits to the system. This is mainly because, in practice, the inherent temporal mismatch between renewable generation and customers' load demand could lead to the inefficient exploitation of renewable energy and high operation cost of the system. However, after DR is introduced, relatively low electricity prices are imposed during off-peak hours, which incentivizes consumers to shift their heating demand to electric heating, resulting in reductions in power generation from CHP and electricity imported from the external market. As such, in this case, the utilization of wind power could increase, which makes the total operation cost of the system decreases accordingly.

Next, we move on the results between Group-2 and our method. As can be seen, the total cost with respect to the suggested solution in Group-2 is much lower than that of the proposed one. This implies that considering the existence of demand-side uncertainties could partially offset the benefits created by deterministic DR and make the contribution of DR program less pronounced in actual implementations.

In other words, the optimal planning solution derived based on the deterministic DR modeling approach might be not necessarily effective in the actual implementation. To reveal this, we then make a further comparison by conducting a hypothesis analysis proposed in (Zeng et al., 2021) to examine the applicability of these two kinds of methods. Specifically, it is assumed that the actual DR capacity achievable by system customers is an uncertain value duration operation and follows a Gaussian distribution with a mean equal to their forecasted value and a standard deviation set to 20% of the mean. Then, we make a comparison for the actual performance of the two planning schemes (i.e., the deterministic solution and the proposed solution) by assessing their regret value (RV) in such uncertain environment. The description about RV and its calculation method can be found in detail in (Zeng et al., 2021).

The calculated values of RV are presented in the last column of Table 11. As observed, although the

deterministic solution (provided by using the methodologies in Group-2) is expected to have a more satisfactory performance during the planning stage, but its RV value is much larger than that of the proposed plan. This indicates that the actual performance of the planning scheme derived from the deterministic method should be less favorable than the proposed solution in the uncertain environment. These results may well prove the superiority of the proposed planning method in actual implementations. In practice, if the decision-maker fails to account for the uncertain nature of DR resources in its decision-making, its resultant planning solution could be not truly optimal, which results in less benefits to the decision-maker than the expected. In contrast, the proposed planning model, due to developed on a stochastic modeling framework, can reproduce actual market functioning and hence it can provide more efficient solutions than the conventional deterministic approach.

Finally, we compare the results between Group-3 and the proposed case. The optimal planning solution has an objective function value of 1867.23 k$ when the correlation among uncertainties are neglected (Group-3), which is larger than that of the proposed case. This phenomenon is mainly due to the fact that the loads cover all locations (buses) and have the much larger capacity value compared to the penetration level of RESs and DR. As such, when considering the effect of these factors together, the inherent correlations existed in their variations would partially change the effect of DR, depending on their respective characteristics. Therefore, in practice, if the potential correlations among these uncertainties existed were neglected from the MES planning formulation, it would lead to an incorrect estimate on the profitability of the investment and hence suboptimal planning decisions. These results indicate that incorporating the correlations among renewable generation, DR, and load demand is important for guaranteeing the effectiveness of MES planning.

Through the above tests, the novelty of the proposed planning framework and its advantages over the existing methods can be clearly presented and justified.

(2) Computational Performance Analysis

In this study, a novel scenario generation and reduction method that can properly address the impact of correlations among uncertainties is employed. To verify the effectiveness of this approach, we conduct a further quantitative study in this section to examine the computational performance of this method with respect to conventional scenario reduction methods used in SP. Two classic scenario reduction techniques, which are referred to as "Dr-distance" (Chen and Yan, 2018) and that based on the traditional similarity function "$Hsim$" (Xie et al., 2010) are considered in this analysis for the purpose of comparison.

The performance of the concerned methods is examined and evaluated from two aspects, namely, *sample stability* and *computational time*. The former criterion is dedicated to indicating the quality of the refined scenario set in terms of statistical consistency with respect to the original solution space, whereas the latter reflects the benefits brought by the applied algorithm, depending on the improvement in solution efficiency.

In this study, the stability of scenario reduction is indicated by using a metric called "out sample stability (OUT)" (Kaut and Wallace, 2003), defined as:

$$OUT(\xi,\tilde{\xi}) = \frac{\left|F^*(x,\xi) - F^*(\tilde{x},\tilde{\xi})\right|}{F^*(x,\xi)} \times 100\% \tag{33}$$

where $F^*(x,\xi)$ is the objective function value obtained by the original scenario set and $F^*(\tilde{x},\tilde{\xi})$ is the objective function value obtained by the reduced scenarios.

The value of OUT reflects the degree of deviation in the objective function value of the solution before and after implementing the scenario reduction. In practice, given a fixed OUT, the algorithm in which fewer scenarios are needed for the approximation of the original dataset is regarded to have better performance.

The relevant results based on different scenario reduction methods are compared and shown in Table 12.

Table 12 Comparison of Different Scenario Reduction Methods

OUT	*Dr*-distance (Chen and Yan, 2018)		*Hsim* (Xie et al., 2010)		*Sim&corrloss*	
	$\tilde{N}_1$	t(s)	$\tilde{N}_1$	t(s)	$\tilde{N}_1$	t(s)
0	500	2710.26	500	2710.26	500	2710.26
2	394	1969.59	349	1776.43	79	328.86
5	169	606.25	138	416.14	18	213.64
10	32	233.38	22	210.44	8	175.95

As can be seen, when the value of OUT is fixed at 2%, 5%, and 10%, the proposed scenario reduction method only requires a smaller number of scenarios to represent the impact of uncertainties, as compared with *Dr*-distance and *Hsim* approach. Moreover, its computational time is also less than the conventional distance-based methods.

Through the above results, it can be seen that the applied scenario reduction method in this paper outweighs the other two reference approaches as discussed. Specifically, it can achieve better performance

in reducing the computational complexity of large-scale SP problems and improving the optimization efficiency, without affecting the quality of the derived solutions. As such, the novelty of the proposed approach and its advantages can be properly justified through this test.

(3) Implement-ability of the Proposed Planning Method

To analyze the implement-ability of the proposed method, a discussion on its adaptability in the context of current market environment is conducted in this section. In this study, the proposed MES planning method corresponds to a centralized approach, which means that it is only suitable and applicable in a centralized market setting. In the centralized environment, all the decisions related in the planning stage, such as the RES sizing and AMI placement, are supposed to be made by the same entity. In reality, the above setting is consistent with most of the distribution-level MES cases in China and many other countries. For example, in China, many distribution-level MES projects take the form of industrial park (Zeng et al., 2020b). A private industrial park owner is responsible for both investment and operation of the MES. In this case, the proposed method can be used as an efficient tool for addressing the MES planning problem. However, it should be noted that, with the deregulation of power and energy sector in the future, a MES might be invested and operated by different market players (e.g., the energy network is owned by the local utility company but renewable energy generation units are owned by a private entity). In this case, the proposed planning approach could be no longer applicable. A game-theoretic optimization framework which takes into account the decision-making of different stakeholders might be a viable option for addressing the MES planning problem in such decentralized context. Thus, this can be counted as a limitation in the applicability of the proposed method for the future market setting.

7. Conclusion

In this paper, a new planning framework utilizing the DR option is presented for enabling CHP-based MESs to accommodate the growing penetration of RESs. As the main novelty of this work, this study examines the potential role of demand response for improving renewable energy exploitation from a long-term planning perspective, instead of the conventional operation aspect. Furthermore, the uncertainties associated with customers' DR performances and their potential correlations with the externalities have also been explicitly considered in this study. The incorporation of DR-related uncertainties into MES planning results in the concerned problem to be a two-stage SP problem, in which the optimal allocation and management of RES generation and demand-side resources (AMI) are determined simultaneously to

minimize the overall economic costs of the system. According to the mathematical feature of the proposed model, an efficient correlation-handled solution approach is used to obtain the final solution to the problem.

The proposed planning framework is demonstrated on an illustrative electricity-thermal interconnected MES test case and the primary conclusions obtained from the case studies are as follows:

1) The operation performance of CHP-based MESs is highly dependent on the load pattern of its customers. As the introduction of DR enables the load consumption to more closely follow the intrinsic supply of RESs, the integrated resource planning model demonstrates a super additive effect, not only in term of lower economic costs but also higher renewable energy utilization.

2) Under the non-direct control-based paradigm, the uncertainties associated with the demand-side responsiveness and its potential correlations with the externalities could have a significant impact on the operational efficiency of DR programs. Therefore, in practice, to ensure the effectiveness/optimality of final planning decisions, such potential correlations among uncertainties should be captured in the planning decision-making of MESs.

3) Compared with conventional distance-based scenario reduction methods, the proposed algorithm, due to proper incorporation of correlations in the probability distribution of uncertainties, can achieve better performance in the SP solution procedures, which makes the derived planning strategy more convincing and reliable in real-world applications.

Acknowledgements

Financial support for this work was provided by the National Natural Science Foundation of China (51507061) and the Chinese National Funding of Social Sciences (19ZDA081).

References

Andersen, A.N., Lund, H., 2007. New CHP partnerships offering balancing of fluctuating renewable electricity productions. J. Clean. Prod. https://doi.org/10.1016/j.jclepro.2005.08.017

Bahrami, S., Sheikhi, A., 2016. From demand response in smart grid toward integrated demand response in smart energy hub. IEEE Trans. Smart Grid 7, 650–658. https://doi.org/10.1109/TSG.2015.2464374

Batel, S., Devine-Wright, P., Tangeland, T., 2013. Social acceptance of low carbon energy and associated infrastructures: A critical discussion. Energy Policy 58, 1–5. https://doi.org/10.1016/j.enpol.2013.03.018

Benam, M.R., Madani, S.S., Alavi, S.M., Ehsan, M., 2015. Optimal configuration of the CHP system using stochastic programming. IEEE Trans. Power Deliv. https://doi.org/10.1109/TPWRD.2014.2356481

Chen, Y., Deng, C., Yao, W., Liang, N., Xia, P., Cao, P., Dong, Y., Zhang, Y., Liu, Z., Li, D., Chen, M., Peng, P., 2019. Impacts of stochastic forecast errors of renewable energy generation and load demands on microgrid operation. Renew. Energy. https://doi.org/10.1016/j.renene.2018.09.110

Chen, Z., Yan, Z., 2018. Scenario tree reduction methods through clustering nodes. Comput. Chem. Eng. https://doi.org/10.1016/j.compchemeng.2017.10.017

Dagher, L., 2012. Natural gas demand at the utility level: An application of dynamic elasticities. Energy Econ. https://doi.org/10.1016/j.eneco.2011.05.010

Dolatabadi, A., Mohammadi-Ivatloo, B., 2017. Stochastic risk-constrained scheduling of smart energy hub in the presence of wind power and demand response. Appl. Therm. Eng. 123, 40–49. https://doi.org/10.1016/j.applthermaleng.2017.05.069

Dupačová, J., Gröwe-Kuska, N., Römisch, W., 2003. Scenario reduction in stochastic programming: An approach using probability metrics. Math. Program. Ser. B. https://doi.org/10.1007/s10107-002-0331-0

Eissa, M.M., 2019. Developing incentive demand response with commercial energy management system (CEMS) based on diffusion model, smart meters and new communication protocol. Appl. Energy. https://doi.org/10.1016/j.apenergy.2018.11.083

Gan, L., Li, G., Zhou, M., 2016. Coordinated planning of large-scale wind farm integration system and regional transmission network considering static voltage stability constraints. Electr. Power Syst. Res. https://doi.org/10.1016/j.epsr.2016.03.002

Gu, W., Lu, S., Wang, J., Yin, X., Zhang, C., Wang, Z., 2017. Modeling of the heating network for multi-district integrated energy system and its operation optimization. Zhongguo Dianji Gongcheng Xuebao/Proceedings Chinese Soc. Electr. Eng. https://doi.org/10.13334/j.0258-8013.pcsee.160991

Heitsch, H., Römisch, W., 2003. Scenario reduction algorithms in stochastic programming. Comput. Optim. Appl. https://doi.org/10.1023/A:1021805924152

Henrion, R., Küchler, C., Römisch, W., 2009. Scenario reduction in stochastic programming with respect to discrepancy distances. Comput. Optim. Appl. https://doi.org/10.1007/s10589-007-9123-z

Henrion, R., Römisch, W., 2018. Problem-based optimal scenario generation and reduction in stochastic programming. Math. Program. https://doi.org/10.1007/s10107-018-1337-6

Jangamshetti, S.H., Guruprasada Rau, V., 2001. Optimum siting of wind turbine generators. IEEE Trans. Energy Convers. https://doi.org/10.1109/60.911396

Hu, J., Li, H., 2019. A new clustering approach for scenario reduction in multi-stochastic variable programming. IEEE Trans. Power Syst. 34, 3813–3825. https://doi.org/10.1109/TPWRS.2019.2901545

Karaki, S.H., Chedid, R.B., Ramadan, R., 1999. Probabilistic performance assessment of autonomous solar-wind energy conversion systems. IEEE Trans. Energy Convers. https://doi.org/10.1109/60.790949

Kaut, M., Wallace, S., 2003. Evaluation of scenario-generation methods for stochastic programming 3, 0–15.

Kim, Y., Norford, L.K., 2017. Optimal use of thermal energy storage resources in commercial buildings through price-based demand response considering distribution network operation. Appl. Energy 193, 308–324. https://doi.org/10.1016/j.apenergy.2017.02.046

Labandeira, X., Labeaga, J.M., López-Otero, X., 2017. A meta-analysis on the price elasticity of energy demand. Energy Policy 102, 549–568. https://doi.org/10.1016/j.enpol.2017.01.002

Linna, N., Changsen, F., Wen, F., Salam, A., 2007. Optimal power flow of multiple energy carriers. IEEE Trans. Power Syst. 22, 145–155. https://doi.org/doi.org/10.1109/TPWRS.2006.888988

Liu, N., He, L., Yu, X., Ma, L., 2018a. Multiparty energy management for grid-connected microgrids with heat- and electricity-coupled demand response. IEEE Trans. Ind. Informatics. https://doi.org/10.1109/TII.2017.2757443

Liu, X., Wu, J., Jenkins, N., Bagdanavicius, A., 2016. Combined analysis of electricity and heat networks. Appl. Energy. https://doi.org/10.1016/j.apenergy.2015.01.102

Liu, Y., Yu, N., Wang, W., Guan, X., Xu, Z., Dong, B., Liu, T., 2018b. Coordinating the operations of smart buildings in smart grids. Appl. Energy 228, 2510–2525. https://doi.org/10.1016/j.apenergy.2018.07.089

Luan, W., 2009. Advanced Metering Infrastructure. Southern Power System Technology 3, 6–10. https://doi.org/10.13648/j.cnki.issn1674-0629.2009.02.021

Mehrjerdi, H., 2020. Dynamic and multi-stage capacity expansion planning in microgrid integrated with electric vehicle charging station. J. Energy Storage 29, 101351. https://doi.org/10.1016/j.est.2020.101351

Mehrjerdi, H., Hemmati, R., 2020. Energy and uncertainty management through domestic demand response in the residential building. Energy 192, 116647. https://doi.org/10.1016/j.energy.2019.116647

Mehrjerdi, H., Rakhshani, E., 2019. Correlation of multiple time-scale and uncertainty modelling for renewable energy-load profiles in wind powered system. J. Clean. Prod. 236, 117644. https://doi.org/10.1016/j.jclepro.2019.117644

Neyestani, N., Yazdani-Damavandi, M., Shafie-Khah, M., Chicco, G., Catalão, J.P.S., 2015. Stochastic modeling of multienergy carriers dependencies in smart local networks with distributed energy resources. IEEE Trans. Smart Grid 6, 1748–1762. https://doi.org/10.1109/TSG.2015.2423552

Pan, G., Gu, W., Wu, Z., Lu, Y., Lu, S., 2019. Optimal design and operation of multi-energy system with load aggregator considering nodal energy prices. Appl. Energy 239, 280–295. https://doi.org/10.1016/j.apenergy.2019.01.217

Papadimitriou, C.N., Anastasiadis, A., Psomopoulos, C.S., Vokas, G., 2019. Demand response schemes in energy hubs: A comparison study. Energy Procedia 157, 939–944. https://doi.org/10.1016/j.egypro.2018.11.260

Pazouki, S., Haghifam, M.R., 2016. Optimal planning and scheduling of energy hub in presence of wind, storage and demand response under uncertainty. Int. J. Electr. Power Energy Syst. 80, 219–239. https://doi.org/10.1016/j.ijepes.2016.01.044

Press, W.H., Teukolsky, S.A., Vettering, W.T., Flannery, B.P., 2007. Numerical recipes the art of scientific computing (Third Edition), CAMBRIDGE UNIVERSITY PRESS. https://doi.org/10.1017/CBO9781107415324.004

Qadrdan, M., Cheng, M., Wu, J., Jenkins, N., 2017. Benefits of demand-side response in combined gas and electricity networks. Appl. Energy. https://doi.org/10.1016/j.apenergy.2016.10.047

Qin, Z., Li, W., Xiong, X., 2013a. Incorporating multiple correlations among wind speeds, photovoltaic powers and bus loads in composite system reliability evaluation. Appl. Energy. https://doi.org/10.1016/j.apenergy.2013.04.045

Qin, Z., Li, W., Xiong, X., 2013b. Generation system reliability evaluation incorporating correlations of wind speeds with different distributions. IEEE Trans. Power Syst. https://doi.org/10.1109/TPWRS.2012.2205410

Rastegar, M., Fotuhi-Firuzabad, M., Lehtonen, M., 2015. Home load management in a residential energy hub. Electr. Power Syst. Res. 119, 322–328. https://doi.org/10.1016/j.epsr.2014.10.011

Shao, C., Ding, Y., Wang, J., Song, Y., 2018. Modeling and integration of flexible demand in heat and electricity integrated energy system. IEEE Trans. Sustain. Energy 9, 361–370. https://doi.org/10.1109/TSTE.2017.2731786

Sheikhi, A., Bahrami, S., Ranjbar, A.M., 2015. An autonomous demand response program for electricity and natural gas networks in smart energy hubs. Energy 89, 490–499. https://doi.org/10.1016/j.energy.2015.05.109

Sheikhi, A., Rayati, M., Ranjbar, A.M., 2016. Demand side management for a residential customer in multi-energy systems. Sustain. Cities Soc. 22, 63–77. https://doi.org/10.1016/j.scs.2016.01.010

Wang, J., Zhong, H., Ma, Z., Xia, Q., Kang, C., 2017. Review and prospect of integrated demand response in the multi-energy system. Appl. Energy. https://doi.org/10.1016/j.apenergy.2017.05.150

Woo, C.K., Liu, Y., Zarnikau, J., Shiu, A., Luo, X., Kahrl, F., 2018. Price elasticities of retail energy demands in the United States: New evidence from a panel of monthly data for 2001–2016. Appl. Energy 222, 460–474. https://doi.org/10.1016/j.apenergy.2018.03.113

Xie, M., Guo, J., Zhang, H., Chen, K., 2010. Research on the similarity measurement of high dimensional data 92–96.

Zeng, B., Dong, H., Sioshansi, R., Xu, F., Zeng, M., 2020a. Bi-Level robust optimization of electric vehicle charging stations with distributed energy resources. IEEE Trans. Ind. Appl. 56 (5), 5836-5847. https://doi.org/10.1109/TIA.2020.2984741

Zeng, B., Zhu, Z., Xu, H., Dong, H., 2020b. Optimal public parking lot allocation and management for efficient PEV accommodation in distribution systems. IEEE Trans. Ind. Appl. 56 (5), 5984-5994. https://doi.org/10.1109/TIA.2020.2986980

Zeng, B., Feng, J., Liu, N., Liu, Y., 2021. Co-optimized parking lot placement and incentive design for promoting PEV integration considering decision-dependent uncertainties. IEEE Trans. Ind. Informatics 17 (3), 1863-1872. https://doi.org/10.1109/TII.2020.2993815

Zeng, B., Zhang, J., Yang, X., Wang, J., Dong, J., Zhang, Y., 2014. Integrated planning for transition to low-carbon distribution system with renewable energy generation and demand response. IEEE Trans. Power Syst. 29 (3), 1153-1165. https://doi.org/10.1109/TPWRS.2013.2291553

Zeng, B., Zhu, X., Chen, C., Hu, Q., Zhao, D., Liu, J., 2019. Unified probabilistic energy flow analysis for electricity-gas coupled systems with integrated demand response. IET Gener. Transm. Distrib. 13 (13), 2697-2710. https://doi.org/10.1049/iet-gtd.2018.6877

Zhang, S., Cheng, H., Li, K., Tai, N., Wang, D., Li, F., 2018. Multi-objective distributed generation planning in distribution network considering correlations among uncertainties. Appl. Energy 226, 743–755. https://doi.org/10.1016/j.apenergy.2018.06.049

Zhang, S., Cheng, H., Zhang, L., Bazargan, M., Yao, L., 2013. Probabilistic evaluation of available load supply capability for distribution system. IEEE Trans. Power Syst. https://doi.org/10.1109/TPWRS.2013.2245924

Zhang, X., Che, L., Shahidehpour, M., Alabdulwahab, A., Abusorrah, A., 2016a. Electricity-natural gas operation planning with hourly demand response for deployment of flexible ramp. IEEE Trans. Sustain. Energy. https://doi.org/10.1109/TSTE.2015.2511140

Zhang, X., Shahidehpour, M., Alabdulwahab, A., Abusorrah, A., 2016b. Hourly electricity demand response in the stochastic day-ahead scheduling of coordinated electricity and natural gas networks. IEEE Trans. Power Syst. https://doi.org/10.1109/TPWRS.2015.2390632

Zhang, Y., Huang, Z., Zheng, F., Zhou, R., An, X., Li, Y., 2020. Interval optimization based coordination scheduling of gas–electricity coupled system considering wind power uncertainty, dynamic process of natural gas flow and demand response management. Energy Reports. https://doi.org/10.1016/j.egyr.2019.12.013